RESEARCH ARTICLE-MECHANICAL ENGINEERING

The Combined Effect of Al$_2$O$_3$ Nanofluid and Coiled Wire Inserts in a Flat-Plate Solar Collector on Heat Transfer, Thermal Efficiency and Environmental CO$_2$ Characteristics

B. Saleh[1] · L. Syam Sundar[2] · Ayman A. Aly[1] · E. Venkata Ramana[3] · K. V. Sharma[4] · Asif Afzal[5] · Yasser Abdelrhman[6] · Antonio C. M. Sousa[2]

Abstract

The present study experimentally investigated the thermal efficiency, collector area, weight, embodied energy, environmental CO$_2$ emissions of Al$_2$O$_3$/water nanofluid flow in a flat-plate solar collector and with coiled wire turbulators. The experiments were performed at ϕ that is equal to 0.1%, 0.2% and 0.3% and volume flow rate from 120 to 300 L/h. Results indicate that the collector thermal efficiency increased with the increase of particle volume loadings and volume flow rates. The thermal efficiency of the collector with water circulate is 53%, whereas it is enhanced to 65% at $\phi = 0.3\%$ nanofluid, and it is further enhanced to 77% for $\phi = 0.3\%$ nanofluid with 10-mm coiled wire insert in a collector tube at a volume flow rate of 300 L/h. The collector area is declined to 8.66% ($\phi = 0.1\%$), 14% ($\phi = 0.2\%$) and 18.66% ($\phi = 0.3\%$) for nanofluids. The collector area is further reduced to 31.33% for $\phi = 0.3\%$ nanofluid and with a coiled wire pitch of 10 mm. The materials embodied energy is decreased to 1144.36 MJ for $\phi = 0.3\%$ nanofluid, and it is further reduced to 1022.6 MJ with the use of a wire coil pitch of 10 mm, but for water, it is 1451.4 MJ. The Nusselt number is increased to 23.22% with $\phi = 0.3\%$ nanofluid, and it further enhanced to 53.56% at same particle loadings and coiled wire pitch of 10 mm over the water data.

Keywords Energy assessment · Environmental · Nanofluid · Wire coil inserts · Turbulator · Economic effect

List of Symbols

A_c	Collector surface area (m^2)
c_p	Heat capacity (J/kg K)
$c_{p,bf}$	Specific heat of base fluid (J/kg K)
$c_{p,np}$	Specific heat of nanoparticles (J/kg K)
$c_{p,nf}$	Specific heat of nanofluid (J/kg K)
d	Tube diameter (m)
d_h	Hydraulic diameter (m)
d_c	Coiled wire diameter (m)
e	Wire thickness (m)
F_R	Heat removal factor
G_T	Global solar radiation (W/m^2)
$\dot{m}$	Mass flow rate (kg/s)
Nu	Nusselt number
P	Pitch (m)
Pr	Prandtl number
$\dot{Q}_u$	Useful energy gained rate (W)
Re	Reynolds number
T_a	Ambient temperature (K)
T_i	Fluid inlet temperature (K)
T_o	Fluid outlet temperature (K)
U_L	Overall heat loss coefficient (W/m^{2}K)
W	Weight (g)

✉ B. Saleh
b.saleh@tu.edu.sa; bahaa_saleh69@yahoo.com

1   Mechanical Engineering Department, College of Engineering, Taif University, P.O. Box 11099, Taif 21944, Saudi Arabia

2   Department of Mechanical Engineering, Centre for Mechanical Technology and Automation (TEMA–UA), University of Aveiro, 3810-193 Aveiro, Portugal

3   I3N, Department of Physics, University of Aveiro, 3810-193 Aveiro, Portugal

4   Department of Mechanical Engineering, Jawaharlal Nehru Technological University-Hyderabad, Hyderabad, India

5   Department of Mechanical Engineering, P. A. College of Engineering, Mangaluru, India

6   Department of Mechanical Engineering, Faculty of Engineering, Assiut University, Assiut 71515, Egypt

🖄 Springer

Greek Symbols

Tα	Absorptance–transmittance product
P	Density (kg/m^3)
Δ	Particle size (nm)
B(2θ)	Half-maximum intensity peak (radians)
θ	Maximum intensity peak angle
T	Solar collector time constant (min)
μ	Viscosity (mPa s)
η_i	Instantaneous collector efficiency
Φ	Particle volume concentration (%)

Abbreviations

CNT	Carbon nanotubes
EG	Ethylene glycol
MWCNT	Multi-walled carbon nanotubes
SDBS	Sodium dodecylbenzene sulfonate

1 Introduction

Climate change is caused due to the CO_2 emissions released by the burning of fossil fuels, which leads to a significant effort for finding various renewable energy sources. Among these renewable energy sources, solar energy plays an increasingly important role and its abundant availability. The storage of solar energy in a working fluid, in the form of heat, is utilized in heating or cooling applications. The flat-plate collector is one of the best examples to store heat in the fluid in which majorly water is used, but with water, proper performance augmentation is not achieved. Replacing the water with nanofluids may achieve augmentation in performance [1].

The use of nanofluids in solar flat-plate collectors has been extensively investigated for quite some time up to date. In early investigations, Yousefi et al. [2, 3] presented nanofluids in a collector using MWCNT/water and Al_2O_3 nanofluids, where an enhancement of 28.3% with 0.2 wt% of Al_2O_3/water nanofluid in the plain collector was reported. Said et al. [4] explained the effect of pH value on the energy and exergy of collector for Al_2O_3/water nanofluid. Hussein et al. [5] used covalent functioned MWCNT/water nanofluids in the collector and found an efficiency enhancement of 85% at mass flow rate of 4 L/min. Choudhary et al. [6] found an efficiency augmentation of 19.2% at 1 vol% at 60 L/h using 50:50% of EG:W–ZnO nanofluid. Tong et al. [7] considered various nanofluids of Al_2O_3 and CuO for the study of exergy, energy efficiency and entropy generation, and they noticed a maximum exergy efficiency of 56.9% at $\phi = 1.0\%$ for Al_2O_3 and 49.6% at $\phi = 0.5\%$ for CuO nanofluid.

Polvongsri and Kiatsiriroat [8] studied silver/water nanofluids, and Natarajan and Sathish [9] investigated CNT/water nanofluids; both the studies reported increased collector efficiency. Otanicar et al. [10] used various kinds of carbon nanotubes, graphite and silver nanofluids and observed an efficiency enhancement of 5% compared with water data. With the use of PG/W mixture in the collector, Shojaeizadeh et al. [11] have reported an efficiency reduction of 15.68% at a 0.0167 kg/s flow rate. Karami et al. [12] have noticed a 17% efficiency increase using 70:30 W/EG–CuO nanofluid. Kiliç et al. [13] prepared TiO_2/water nanofluids by adding 0.2 wt% of Triton X-100 surfactant and found collector thermal efficiency of 48.67% with the use of 2 wt% of TiO_2/H_2O nanofluids in the collector. Chaji et al. [14] have noticed 3.5% and 10.5% thermal efficiency enhancement in the collector with the use of 0.1 wt% and 0.3 wt% of TiO_2/water nanofluids. Said et al. [15] have expressed energy and exergy enhancement based on the Al_2O_3 nanofluid. Zamzamian et al. [16] have expressed a maximum of 45% decrease in $F_R U_L$ parameter employing Cu/EG in the collector at $\phi = 0.3\%$ with 1 lit/min flow rate. Based on TiO_2/water nanofluid, Said et al. [17] have achieved a collector thermal efficiency of 76.6% at 0.1 wt% and at a 1.5 kg/min flow rate. In a similar manner, MWCNT/water nanofluid was used by Sabiha et al. [18] and presented 93.43% efficiency at $\phi = 0.2\%$ and 0.025 kg/s flow rate. Jouybari et al. [19] investigated the efficiency using SiO_2/water nanofluid and observed improvement in efficiency up to 73% at 0.6% particle loading. The detailed analyses employing nanofluids in the collector have been reviewed by Mahian et al. [20] and Javadi et al. [21]. The literature related to the utilization of nanofluids in a flat-plate collector is summarized in Table 1.

The collector tubes by adding wire coil configurations can provide further efficiency enhancements. The wire coil configurations were studied by Garcia et al. [22] by considering W/PG fluid in a horizontal tube. They performed experiments at different Re values (80–90,000), Pr values (2.8–150), pitch/diameter ratios (1.18 < p/d < 2.68) and pitch space to diameter ratios (0.07 < e/d < 0.10). In another study, Garcia et al. [23, 24] performed experiments for W/PG fluid in a tube at Re ranging from 10 to 2500 and Pr ranging from 200 to 700. For the case of Fe_3O_4 nanofluids, Sundar et al. [25] have observed 32.03% Nusselt number enhancement at particle loadings of 0.06% with coiled wire pitch to diameter ratio of 1 at Reynolds number of 30,000. With the use of TiO_2–SiO_2 nanofluid and coiled wire pitch to diameter, the ratio is 4.17, and Hamid et al. [26] presented Nusselt number enhancement of 254.4% at $\phi = 3.0\%$ and Reynolds number of 12,000. Goudarzia and Jamalia [27] have obtained Nusselt number, and thermal performance augments to 9% and 5% employing Al_2O_3/EG and coiled wire inserts at $\phi = 1\%$. Akyürek et al. [28] have obtained a remarkable Nusselt number increase with the use of coiled wire

Table 1 Summary of literature investigations reported the effect of different nanofluids on the collector efficiency

Author	Nanofluids	Concentrations	Efficiency enhancement
Yousefi et al. [3]	Al_2O_3/water	0.2%	28.3%
Hussein et al. [5]	f-MWCNT/water		85%
Choudhary et al. [6]	ZnO/50:50 EG:W	1%	69.24%
Tong et al. [7]	Al_2O_3/water, CuO/water	1.0%, 0.5%	Exergy efficiency of 56.9% and 49.6%
Otanicar [8]	CNT/water, Graphite/water Silver/water		5%
Karami et al. [12]	70:30 W:EGCuO		9–17%
Kiliç et al. [13]	TiO_2/water	0.2%	48.67%
Chaji et al. [14]	TiO_2/water	0.1%, 0.3%	3.5% 10.5%
Zamzamian et al. [16]	Cu/EG	0.3%	Decrease of $F_R U_L$ parameter up to 45%
Said et al. [17]	TiO_2/water	0.1%	76.6%
Sabiha et al. [19]	SWCNT/water	0.2%	Exergy efficiency of 93.43% and thermal efficiency of 26.25%
Jouybari et al. [13]	SiO_2/water	0.6%	73%

inserts in a double-pipe concentric tube heat exchanger utilizing Al_2O_3/water nanofluids.

The use of inserts of twisted tape and longitudinal strip in the collector with nanofluid may provide additional collector performance. For Al_2O_3/water nanofluid in the collector with twisted-type tape insert of $H/D = 5$ showed 76% efficiency of the collector, and using a longitudinal strip insert of AR = 1 efficiency of 82% for the collector efficiency was reported by Sundar et al. [29, 30]. However, their analyses did not include the collector area, cost, weight and environmental aspects.

Experimental investigation of nanofluid circulating in the collector utilizing various pitches of coiled wire configurations is not presented in the literature; therefore, the current work is undertaken to analyze the efficiency, embodied energy, cost, weight, environmental aspects and heat transfer by experimental means. The obtained values are validated with the literature. From the data, valid regression equations for Nusselt number and friction factor are presented. Combining both surface modification techniques and stable working fluids with higher thermal conductivity is limited, and the findings from this study will be useful for the broader scientific community and industry utilizing such techniques for heat transfer enhancement for various heating and cooling applications.

2 Experimental Study

2.1 XRD and SEM Analysis

The XRD (Siemens D-500, 45 kV) and SEM (Hitachi, SU-70) analysis was performed on purchased Al_2O_3 nanoparticles. Figure 1a is the XRD spectra, and Scherrer's equation is used to estimate the particle diameter.

$$\delta = \frac{0.94\lambda}{B(2\theta)\cos\theta} \tag{1}$$

The terms in Eq. (1) are particle size (δ), wavelength (λ), $B(2\theta)$ is the half-maximum intensity peak (radians), and θ is the maximum intensity peak angle.

From XRD spectra, the maximum intensity peak is (220); correspondingly, 2θ value is 32.80°, and $B(2\theta)$ value is 0.29°. By incorporating the above values in Eq. (1) it is found the particle size (δ) of 33.9 nm. The SEM image is displayed in Fig. 1b and found that the nanoparticles are spherical.

2.2 Preparation of Al_2O_3 Nanofluid

The Al_2O_3 nanoparticles (Sigma-Aldrich Chemicals, USA) were dispersed in de-ionized water by adding sodium dodecylbenzene sulfonate ($C_{18}H_{29}NaO_3S$) to distilled water in the particle loadings of 0.1%, 0.2% and 0.3%.
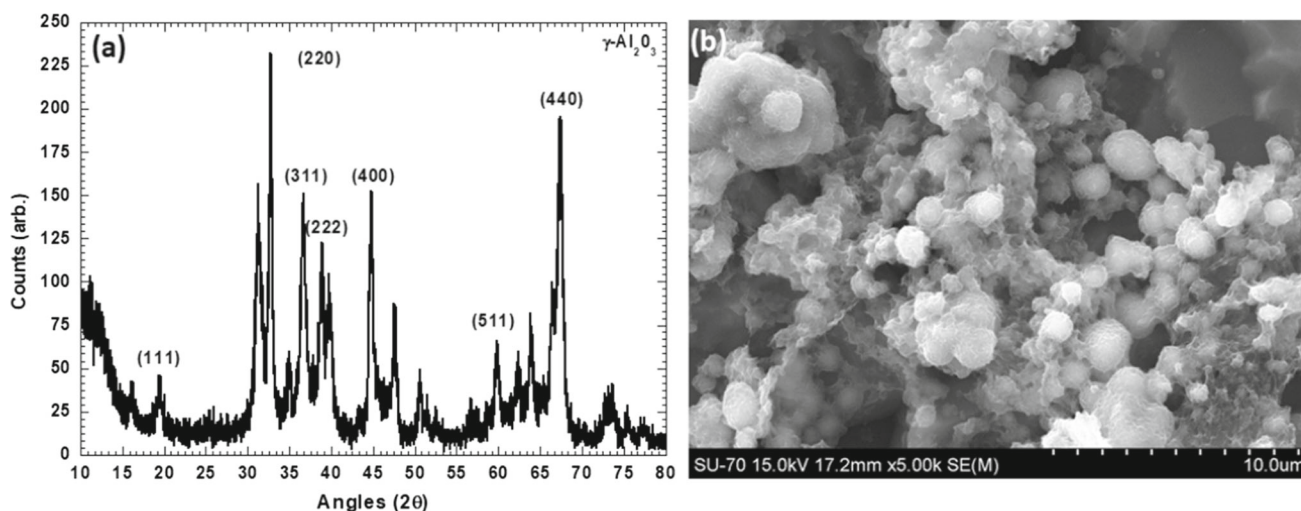
Fig. 1 Al$_2$O$_3$ nanoparticles: **a** XRD patterns, **b** SEM image

$$W_{Al_2O_3} = \frac{\phi \left[\frac{W}{\rho}\right]_w \rho_{Al_2O_3}}{(1 - \phi)} \quad (2)$$

The terms in Eq. (2) are the weight of water ($W = 15$ kg), the density of nanoparticles (3890 kg/m^3), ϕ is particle loadings (%), and $W_{Al_3O_3}$ is the nanoparticles weight, which is calculated.

In 15 l of de-ionized water, the particles of 50.7 g, 100.53 g and 152.4 g were diluted to achieve 0.1%, 0.2% and 0.3% particle loadings. The SDBS of 1/10th (as per the weight of the particles) was used. In the 30 l capacity of the plastic tank, 15 l of water was filled initially, and then the required quantity of surfactant was added and stirred mechanically with low rpm. Then the added required volume concentration of nanoparticles is stirred mechanically at a low speed. The same procedure is used for other nanofluid particle loadings. Figure 2 is the sample (Fig. 2a) and bulk nanofluids during the preparation (Fig. 2b).

The stability of nanofluids was measured utilizing the zeta sizer instrument (Malvern™). The zeta potential of 0.1%, 0.2% and 0.3% nanofluids is found to be − 45.2, − 46.8 and − 41.6 mV at a temperature of 25 °C, − 44.2, − 42.5 and − 39.2 mV at a temperature of 70 °C. It is observed that at higher temperatures, the stability of nanofluids reduced a little and still stayed above 30 mV, which is considered as stable nanofluids, which means that the nanofluids remain stable during the heating and cooling cycles.

The below equations were considered for the evaluation of thermal properties.

1. Pak and Cho [31] equation (ρ and c_P):

$$\rho_{nf} = \phi \rho_p + (1 - \phi) \rho_{bf} \quad (3)$$

Table 2 Properties of Al$_2$O$_3$ nanoparticles and water at 303 K

	ρ (kg/m^3)	k (W/m K)	C_p (J/kg K)	μ (mPa s)
Al$_2$O$_3$	3890	35	880	–
Water	998	0.6129	4180	0.8315

$$c_{p,nf} = \phi c_{p,p} + (1 - \phi) c_{p,bf} \quad (4)$$

2. Einstein [32] model (μ)

$$\mu_{nf} = \mu_{bf}(1 + 2.5\phi) \quad (5)$$

3. Maxwell [33] model (k)

$$k_{nf} = k_{bf} \left[\frac{k_p + 2k_{bf} + 2\phi(k_p - k_{bf})}{k_p + 2k_{bf} - \phi(k_p - k_{bf})} \right] \quad (6)$$

The terms are ϕ is the volume concentration (%), μ is the viscosity (mPa s), and the subscripts are particle (p), base fluid (bf) and nanofluid (nf). Table 2 reports the Al$_2$O$_3$ and water properties, and Table 3 indicates the thermal properties of nanofluids.

2.3 Components

The water or nanofluid tank, fluid flow meter, pressure valves, pump and data logger were utilized. The collector was purchased from Sunlight Solar Systems, India, with an area of 3 m^2. The arrangement of parts line diagram is presented in Fig. 3, the image of collector and tank is given in Fig. 4a, b, and the dimensions are shown in Fig. 5a. The specifications are listed in Table 4. The collector is located outdoor with a tilt of 28°. Measuring atmospheric, fluid (inlet and outlet)

Fig. 2 Preparation of Al_2O_3 nanofluids (**a**) sample and (**b**) bulk nanofluid
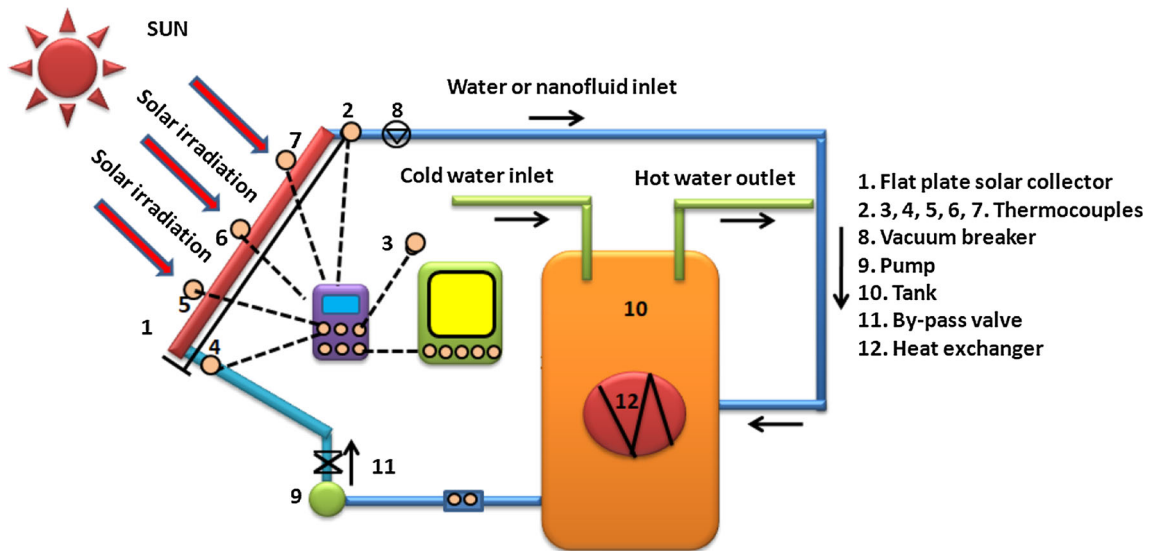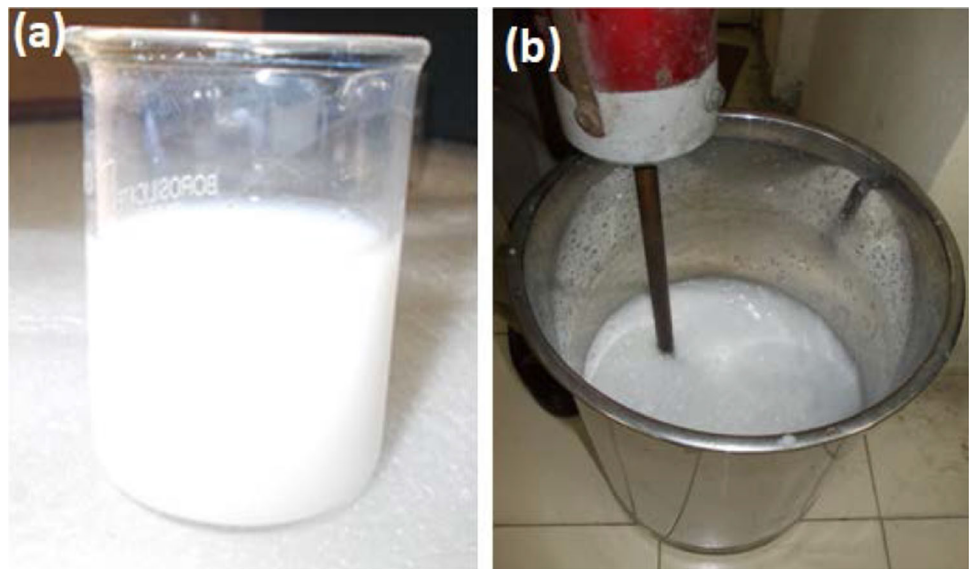
Fig. 3 Schematic diagram of the experimental solar flat-plate collector

**Table 3** The thermophysical properties of Al_2O_3 nanofluids at 303 K and 343 K

Temperature		ρ (kg/m^3)	k (W/m K)	c_p(J/kg K)	μ (mPa s)
303.0 K	Water	998	0.613	4178	0.832
	0.1	1000	0.617	4175	0.834
	0.2	1003	0.622	4172	0.836
	0.3	1006	0.629	4168	0.841
343.0 K	Water	980	0.664	4188	0.389
	0.1	983	0.669	4185	0.397
	0.2	986	0.673	4181	0.391
	0.3	989	0.681	4178	0.392

and surface temperatures by six Pt-100 resistance thermometers, the pressure gauge was utilized to measure the pressure through the tube. The temperatures are connected to a computer across a temperature logger. The temperatures were recorded for fluid volume flow rates (water or nanofluid) of 120, 180, 240 and 300 L/h.

2.4 Wire Coil Inserts

The wire coils inserted collector diagram is shown in Fig. 5a, and the image of coiled wire configurations is placed in Fig. 5b. The wire coil inserts were made with spring steel (EN 42J) material of 1.5 mm diameter, which is turned to the coiled wire with pitches of 10, 13.4, 17.9 mm. In each riser
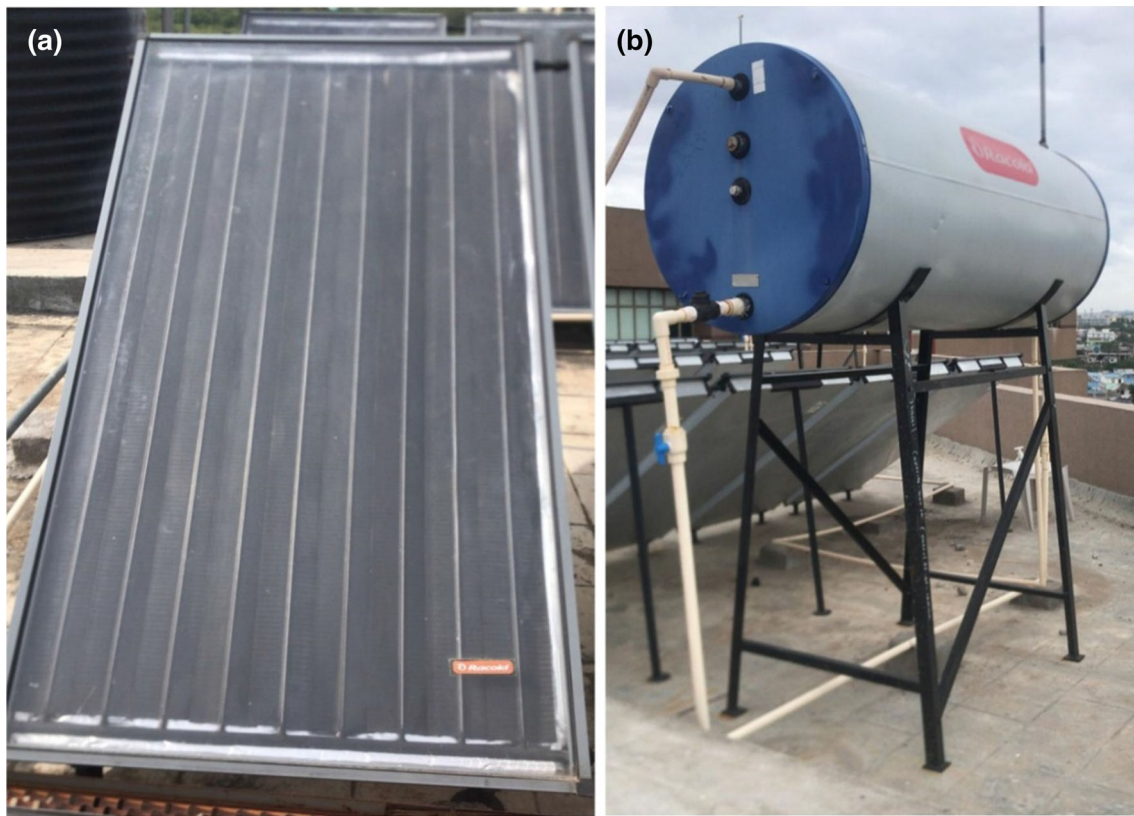
Fig. 4 Photograph of the solar flat-plate collector (**a**) and tank (**b**)

tube, a coiled wire insert is added. A photograph of the wire coil inserts is shown in Fig. 5c.

2.5 Procedure

The tank is filled with the working fluid (water/nanofluids), which circulated with the aid of a pump at flow rates of 120, 180, 240 and 300 L/h. With inner tube diameter (d) and hydraulic diameter (d_h) the Re values are estimated (Re $= 4\dot{m}/\pi d \mu$) and (Re $= 4\dot{m}/\pi d_h \mu$). The coiled wire configurations are noted in Table 5.

$$\text{Hydraulic diameter,} \quad d_h = \frac{d^2 - \left(\frac{\pi e^2 d_c}{p}\right)}{d + \left(\frac{\pi e d_c}{p}\right)} \tag{7}$$

The terms in Eq. (7) are pitch (p), tube diameter (d), coiled wire diameter (d_c) and coiled wire thickness (e).

Based on d_h values, and at the same Re for nanofluids with coiled wire inserts, the fluid flow rate is adjusted based on the below equation.

$$\dot{m} = \text{Re} \times \pi d_h \mu/4. \tag{8}$$

2.6 Uncertainty Analysis

The uncertainties associated with the experimental measurements are analyzed from the below equation:

$$U_y^2 = \sum_{i=1}^{n} U_{x,i}^2 \tag{9}$$

The terms in Eq. (9) are uncertainty (U_y) and root-sum-square ($U_{x,i}$) of the measured parameter.

The efficiency (U_η) uncertainty is shown in the below equation.

$$(U_\eta)^2 = \left(\frac{\Delta \dot{m}}{\dot{m}}\right)^2 + \left(\frac{\Delta (T_o - T_i)}{T_o - T_i}\right)^2 + \left(\frac{\Delta G_T}{G_T}\right)^2 \tag{10}$$

The calculated values from Eq. (10) are indicated in Table 6.
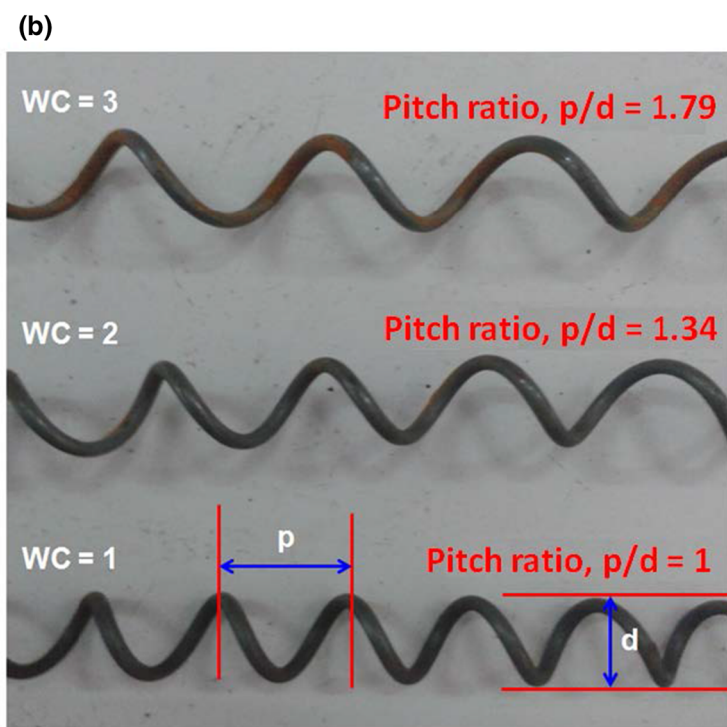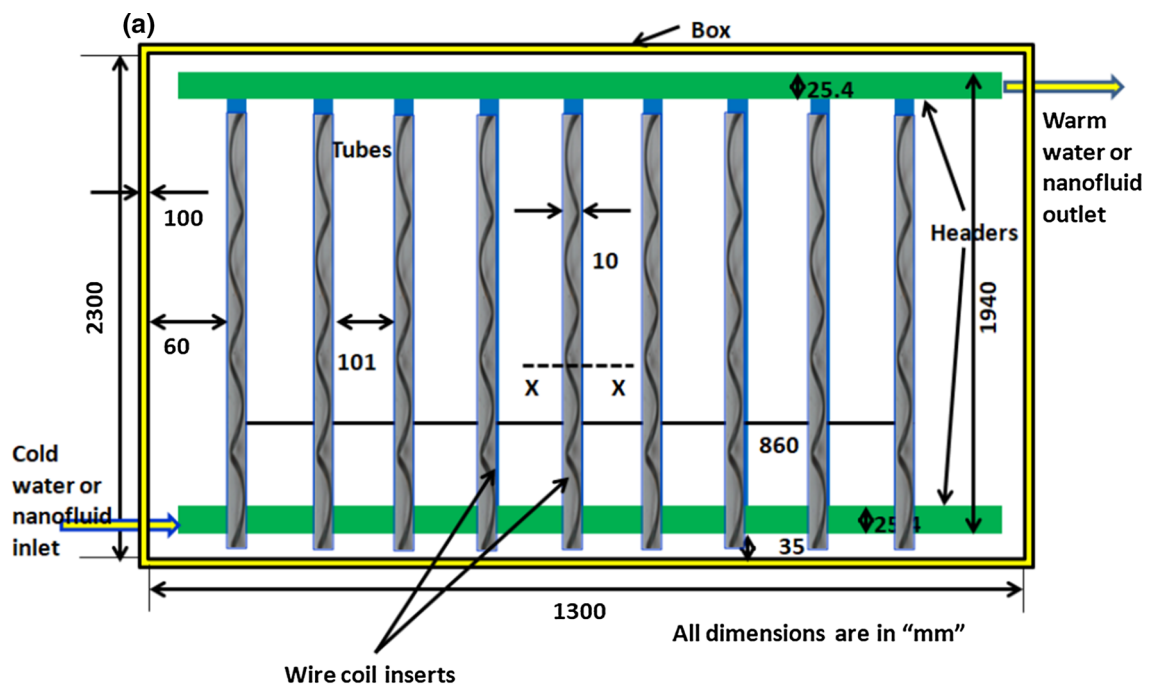
(a)

(b)

Fig. 5 Solar flat-plate collector **a** wire coil inserted in all the tubes along with dimensions, **b** photograph of wire coil inserts

3 Results and Discussion

3.1 Efficiency

The test conditions were performed through ASHRAE standards 93-2003 [34], and the values are presented in Table 7. The below equations are used for evaluating the collector efficiency.

$$Q_u = \dot{m} C_p (T_o - T_i) \tag{11}$$

$$Q_u = A_c F_R [G_T \tau \alpha - U_L (T_i - T_a)] \tag{12}$$

Table 4 Specifications of the solar flat-plate collector

Parameter	Description
Collector area (m^2)	3.0
Absorber plate thickness (mm)	0.6
Inner and outer diameter (mm)	10 and 11
Tube spacing (mm)	0.15
System capacity	120 L
Outlet temperature (°C)	60.0
Coatings of the solar collectors	Selectively coated
Absorber fin, header and riser material	Copper
Glass	Special toughened glass 4 mm thick
Box dimensions (mm)	2030 × 1030 × 100
Aperture size (m^2)	2.0
Risers number	9.0
Size of the header (mm)	25.4
Protrusion inside the header (mm)	2.0
Connecting nuts, bolts and washers	Stainless steel 304
Number of panel boxes	1
Circulation	Forced convection
Storage tank for hot water capacity (liters)	1000
Thickness (mm)	1.2
Density of the tank insulation material (kg/m^3)	48.0
Thickness of the insulation (mm)	100 mm

Table 6 Different parameter uncertainties

S. nos	Parameter	Uncertainty (%)
1	Solar intensity	±3.5%
2	Temperature difference	±1.5%
3	Mass flow rate	±2.5%
4	Area	±2.0%
5	Density	±1.0%

Table 7 The solar collector boundary conditions at the outdoor condition as per ASHRAE 93–2003

Wind speed	2.1–4.3 m/s
Solar radiation	≥ 810 W/m^2
Inlet temperature of the maximum fluid variation	31.1 °C
Maximum variation in flow rate	0.001%
Inlet temperature maximum variation	1 °C

3.1.1 Plain Collector for Nanofluids

The solar insulation engrossed by water and nanofluids working fluids results in different thermal efficiency. The benchmark results of water are shown in Fig. 6a at different analysis values of $(T_i - T_a/G_T)$. If the reduced temperature $(T_i - T_a/G_T)$ is equal to zero, then maximum efficiency by the collector is reached, which indicates that the inlet fluid temperature is equal to ambient temperature $(T_i = T_a)$. When water flows in the collector at flow rates of 120 and 300 L/h, the thermal efficiency reaches up to 46% and 53%. The thermal efficiency of water enhanced with an increase in the flow rate of the fluid.

Later the experiments were performed with nanofluids, and the collector efficiency was evaluated. Figure 6b–d indicate the collector efficiency of nanofluids. When the nanofluid at $\phi = 0.1\%$, 0.2% and 0.3% particle loadings, the efficiencies are 51% and 58%, 53% and 61.5% and 55% and 65%, respectively, at 120 L/h and 300 L/h, by means of percentage 9.43%, 16% and 22.64% in comparison with water. Nanofluids as absorbing fluid in the collector attracted more amounts of heat rather than water, resulting in enhanced efficiency.

The formulated efficiencies data for reaching the parameters of $F_R U_L$ and $F_R \tau \alpha$ are presented in Table 8. With an enhanced fluid flow rate from 120 to 300 L/h, the intersec-

The Hottel–Whillier–Bliss [35–38] equaxtions:

$$\eta_i = \frac{Q_u}{A_c G_T} = \frac{\dot{m} C_p (T_o - T_i)}{G_T} \qquad (13)$$

$$\eta_i = F_R \tau - F_R U_L \left(\frac{T_i - T_a}{G_T} \right) \qquad (14)$$

The terms in Eq. (14) are heat gain (Q_u), flow rate ($\dot{m}$), collector area (A_C), heat removal factor (F_R), absorptance–transmittance ($\tau \alpha$) and solar radiation (G_T) and loss coefficient (U_L).

Table 5 The wire coil inserts characteristic dimensions

Wire coil insert type	d (mm)	d_h (mm)	p (mm)	e (mm)	$\frac{p}{d}$	$\frac{e}{d}$	$\frac{p}{e}$
Plain tube	10	–	–	–	–	–	–
$p/d = 1$	10	6.31	10.0	1.5	1.00	0.15	6.66
$p/d = 1.34$	10	7.01	13.4	1.5	1.34	0.15	8.93
$p/d = 1.79$	10	7.60	17.9	1.5	1.79	0.15	11.93

Table 8 The heat removal factor and absorbed energy parameter values of water and nanofluids at various flow rates

ϕ (%)	Flow rate (L/h)	$F_R U_L$	$F_R \tau \alpha$	R^2
Water	120	− 15.12	0.513	0.997
	180	− 13.26	0.534	0.987
	240	− 11.60	0.545	0.985
	300	− 10.97	0.567	0.995
0.1%	120	− 16.43	0.575	0.991
	180	− 15.95	0.598	0.986
	240	− 14.83	0.627	0.983
	300	− 13.57	0.650	0.978
0.2%	120	− 16.31	0.608	0.993
	180	− 14.39	0.630	0.989
	240	− 13.34	0.664	0.993
	300	− 12.69	0.691	0.979
0.3%	120	− 15.17	0.631	0.993
	180	− 13.67	0.660	0.979
	240	− 13.29	0.703	0.974
	300	− 11.94	0.728	0.986

tion point ($F_R U_L$) is decreased, the slope ($F_R \tau \alpha$) is found to be 0.513 and 0.578 for water, 0.575 and 0.650 for 0.1% nanofluid, 0.608 and 0.691 for 0.2% nanofluid and 0.631 and 728 for 0.3% nanofluid, respectively.

3.1.2 Plain Collector for Water and Wire Coil Configurations

With the use of coiled wire configurations, higher thermal efficiencies were obtained. The water in collector with coiled wire configurations results is shown in Fig. 7a–c at different analysis values of ($T_i - T_a / G_T$). Water with wire coil pitches of 17.9, 13.4 and 10 mm resulted in 57% 62%, and 64% collector efficiencies; however, water without coiled wires showed an efficiency of 53% at 300 L/h flow rate, which in terms of percentage is 7.54%, 16.98% and 20.75%, respectively. Fluid turbulence created by the wire coil inserted in the riser tubes provides higher fluid outlet temperatures. The decreased coiled wire pitch results in augmented efficiencies. The formulated data are seen in Table 9, and the $F_R \tau \alpha$ values are reached to 0.634 and 0.688 and 0.711 for the case of coiled wire pitches of 17.9, 13.4 and 10 mm.

3.1.3 Plain Collector for ϕ = 0.1% and Wire Coil Configurations

After the evaluation of thermal efficiency for water with coiled wire configurations, the nanofluids are used one after another in the collector. The efficiency was evaluated using Eq. (11). At ϕ = 0.1% of nanofluid particle loading with coiled wire configurations, the efficiency data are shown in

Fig. 8a–c and 0.1% particle loadings of nanofluid in plain collector with coiled wire pitches of 17.9, 13.4 and 10 mm, and an efficiency of 64%, 67% and 70% for the collector was obtained; however, for the plain collector (ϕ = 0.1%) efficiency of 58% is obtained at 300 L/h flow rate, which is 10.31%, 15.51% and 20.68%, respectively. The formulated data are seen in Table 9; the $F_R \tau \alpha$ values are reached to 0.726 and 0.748 and 0.796 for the case of coiled wire pitches of 17.9, 13.4 and 10 mm; for plain 0.1% nanofluid a value of 0.650 is obtained.

3.1.4 Plain Collector for ϕ = 0.2% and Wire Coil Configurations

The thermal efficiency of nanofluid with ϕ = 0.2% particle loading with various coiled wire configurations is indicated in Fig. 9a–c. Nanofluid with 0.2% particle loadings in the plain collector and coiled wire pitches of 17.9, 13.4 and 10 mm showed an efficiency enhancement of 68%, 71% and 73.5%; however, for nanofluid with 0.2% volume concentration in the plain collector without coiled wire pitches showed an efficiency of 61.5% at 300 L/h flow rate which is 10.59%, 15.44% and 19.51% higher compared to ϕ = 0.2% nanofluid. The formulated data are seen in Table 10; the $F_R \phi$ values reached to 0.780 and 0.806 and 0.834 for the case of coiled wire pitches of 17.9, 13.4 and 10 mm and nanofluid with ϕ = 0.2% particle loading; however, in the case of ϕ = 0.2% nanofluid only, a value of 0.691 was achieved.

3.1.5 Plain Collector for ϕ = 0.3% and Wire Coil Configurations

The thermal efficiency of nanofluid with ϕ = 0.3% particle loading and various wire coil inserts is displayed in Fig. 10a–c. The thermal efficiency for ϕ = 0.3% nanofluid with coiled wire pitches of 17.9, 13.4 and 10 mm showed an efficiency of 72%, 74% and 77% for the collector, but the plain collector (0.3% particle loading) showed an efficiency of 65% at 300 L/h flow rate which is 10.76%, 13.84% and 18.46% higher compared to 0.3% nanofluid. The formulated data are seen in Table 10; the $F_R \tau \alpha$ values reached to 0.832 and 0.845 and 0.871 for the case of coiled wire pitches of 17.9, 13.4 and 10 mm; in case of the plain collector with nanofluid at ϕ = 0.3% particle loading a value of 0.728 is obtained. With the use of coiled wire pitches from 17.9 to 10 mm, the collector efficiency is augmented, and at the same time, $F_R \phi$ also augmented. Coiled wire configurations create turbulence in the nanofluid flow in the collector, resulting in increased efficiencies.
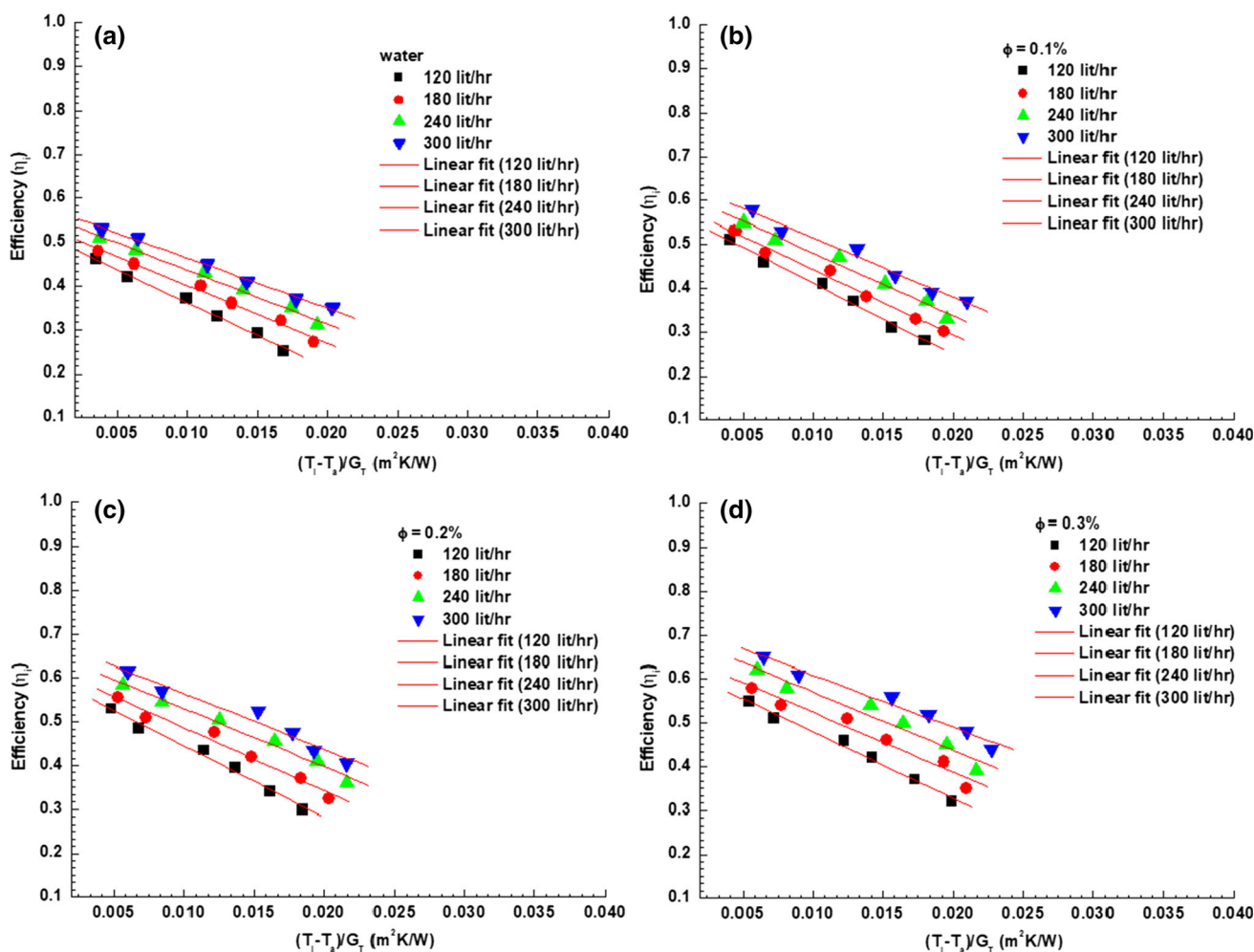
Fig. 6 The collector thermal efficiency as a function of reduced temperature parameter at various volume flow rates: **a** $\phi = 0.0\%$, **b** $\phi = 0.1\%$, **c** $\phi = 0.2\%$ and **d** $\phi = 0.3\%$

3.2 Size Reduction of the Collector's Area

3.2.1 Plain Collector for Nanofluids

The area of the collector from the collector efficiency was analyzed with the increased particle loadings and wire coil inserts, for increased collector efficiency. The equation below is used to calculate the collector's area.

$$\text{Collector area,} \quad A_c = \frac{\dot{m} C_p (T_o - T_i)}{G_T \times \eta_i} \quad (15)$$

$$\text{Mass flow rate,} \quad \dot{m} = \rho \times v \quad (16)$$

The collector thermal efficiency with nanofluids from Fig. 6 indicates increased efficiency. Hence, using the augmented efficiency of the collector, its area is evaluated. In the current investigation, the area is equal to 3 m^2; the same area of the collector is used for other nanofluids. At the fixed mass flow rates and solar radiation, thermal efficiency is increased.

Those values are used for reverse calculation of the collector area. The collector with 0.1%, 0.2% and 0.3% nanofluids showed a reduction in area of 2.74 m^2, 2.58 m^2 and 2.44 m^2, whereas the original area of collector is 3 m^2. The reduced collector area by means of percentage is 8.66%, 14% and 18.66% for particle loadings of $\phi = 0.1\%$, 0.2% and 0.3% nanofluids.

3.2.2 Plain Collector for Nanofluids and Wire Coil Configurations

The enhanced efficiency of the collector was obtained with added coiled wire configurations. The same enhanced efficiency of the collector was used for further collector area calculations. The water with coiled wire pitches of 17.9, 13.4 and 10 mm configurations resulted in reducing the collector area to 2.78, 2.5 and 2.48 m^2, whereas the collector with pure water has an area of 3 m^2. The reduced collector area
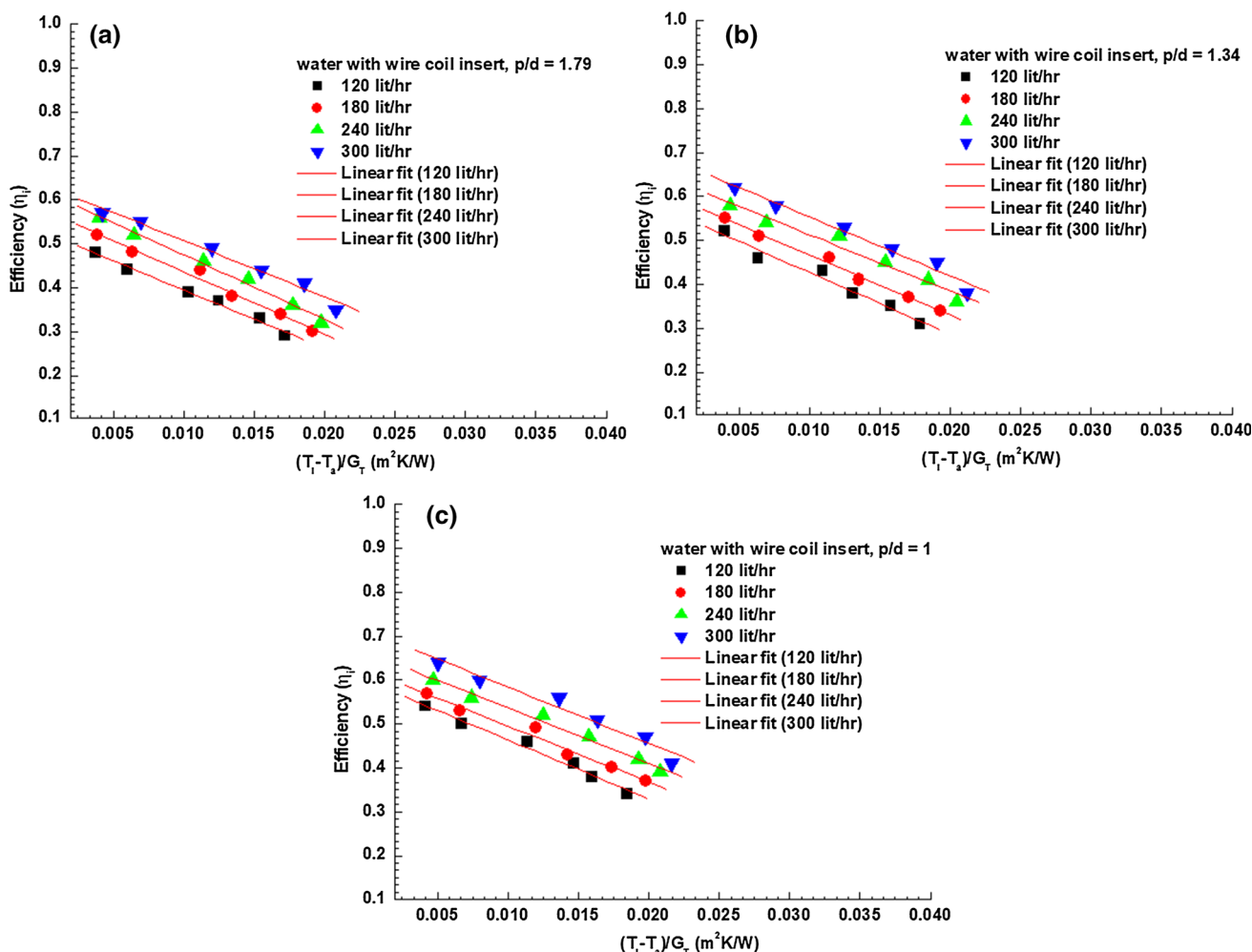
Fig. 7 The collector thermal efficiency with water and different wire coil inserts at various flow rates: **a** $p/d = 1.79$, **b** $p/d = 1.34$, **c** $p/d = 1$

is expressed in terms of percentage, which is 7.33%, 14.66% and 17.33%, respectively.

Moreover, with $\phi = 0.1\%$ particle loading of nanofluid of coiled wire pitches of 17.9, 13.4 and 10 mm configurations, the area of collector decreased to 2.48 m², 2.37 m², 2.27 m², whereas the collector with pure water has an area of 3 m². The reduced collector area is expressed in terms of percentage, which is 17.33%, 21% and 24.33%, respectively.

Meanwhile, the nanofluid with $\phi = 0.2\%$ particle loading and coiled wire pitches of 17.9, 13.4 and 10 mm configurations, the area of collector decreased to 2.33 m², 2.23 m², 2.16 m², whereas the collector using pure water has an area of 3 m². The reduced collector area is expressed in terms of percentage, which is 22.33%, 25.68% and 28%, respectively.

Similarly, the nanofluid with $\phi = 0.3\%$ particle loading and coiled wire pitches of 17.9, 13.4 and 10 mm configurations, the area of collector decreased to 2.20 m², 2.17 m², 2.06 m², whereas the collector with pure water has an area of 3 m². The reduced collector area is expressed in terms of percentage, which is 26.66%, 27.66% and 31.33%, respec-

tively. The area collector decreased employing nanofluids, and coiled wire configurations are noticed in Fig. 11.

3.3 Weight Reduction of Collector

3.3.1 Plain Collector for Nanofluids

The collector weight used in the present study is 50 kg, the breakdown of glass and copper, which is in the order of 38 kg and 12 kg. The results reveal that the collector increased with the increase of particle loadings. For the collector with 0.1% nanofluids, its weight is decreased to 45.68 kg, in which the glass and copper are 34.71 kg and 10.96 kg. However, the collector weight further decreased by adding higher particle loadings. Meanwhile, the collector with 0.2% particle loadings, its weight is 43 kg, in which the glass and copper are 32.68 kg and 10.32 kg. Moreover, the collector with 0.3% particle loadings, its weight decreased to 40.16 kg, in which the glass and copper are 30.90 kg and 9.25 kg. The decreased weight is equal to 8.64%, 14% and 19.68% compared to the

Table 9 The heat removal factor and absorbed energy parameter values of water and 0.1% nanofluid with various wire coil inserts and flow rates

Wire coil inserts type	Flow rate (L/h)	water			$\phi = 0.1\%$		
		$F_R U_L$	$F_R \tau \alpha$	R^2	$F_R U_L$	$F_R \tau \alpha$	R^2
$p/d = 1.79$	120	− 13.23	0.527	0.994	− 17.86	0.618	0.992
	180	− 14.13	0.577	0.991	− 15.70	0.653	0.971
	240	− 14.70	0.621	0.995	− 14.76	0.688	0.982
	300	− 12.79	0.634	0.989	− 14.44	0.726	0.993
$p/d = 1.34$	120	− 14.11	0.568	0.987	− 18.09	0.660	0.990
	180	− 13.67	0.603	0.996	− 16.92	0.691	0.992
	240	− 12.79	0.640	0.982	− 15.23	0.727	0.978
	300	− 13.45	0.688	0.986	− 14.25	0.748	0.997
$p/d = 1$	120	− 13.40	0.597	0.991	− 17.01	0.697	0.970
	180	− 12.73	0.622	0.989	− 15.28	0.717	0.981
	240	− 12.54	0.661	0.993	− 14.20	0.755	0.968
	300	− 12.77	0.711	0.979	− 14.01	0.796	0.982
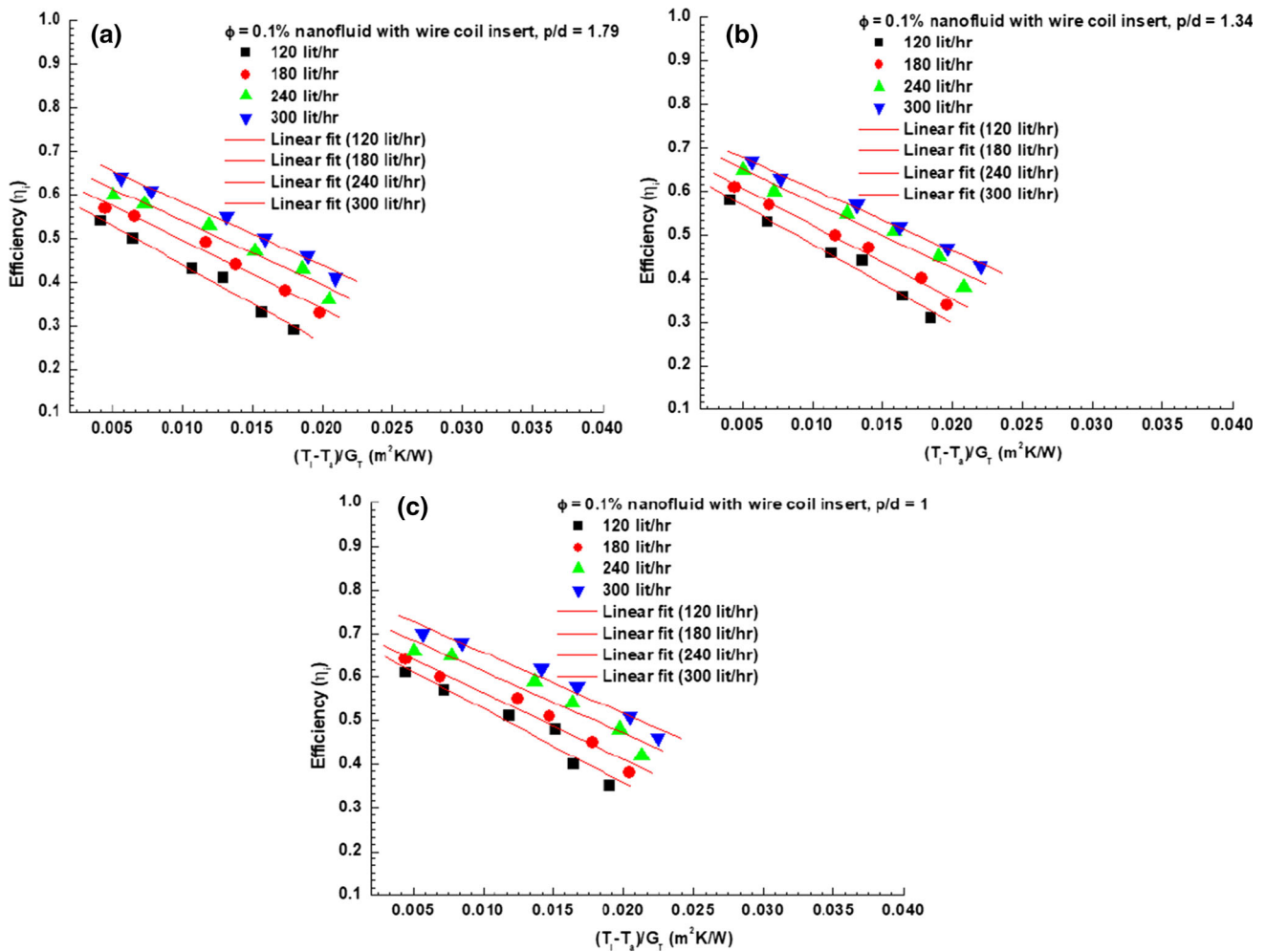
Fig. 8 Thermal efficiency of the collector with $\phi = 0.1\%$ nanofluid and different wire coil inserts at different flow rates: **a** $p/d = 1.79$, **b** $p/d = 1.34$, **c** $p/d = 1$

water collector. To manufacture 100 units of solar collectors working with nanofluids, the decreased collector weight is reached to 432 kg ($\phi = 0.1\%$), 700 kg ($\phi = 0.2\%$) and 984 kg ($\phi = 0.3\%$), respectively.

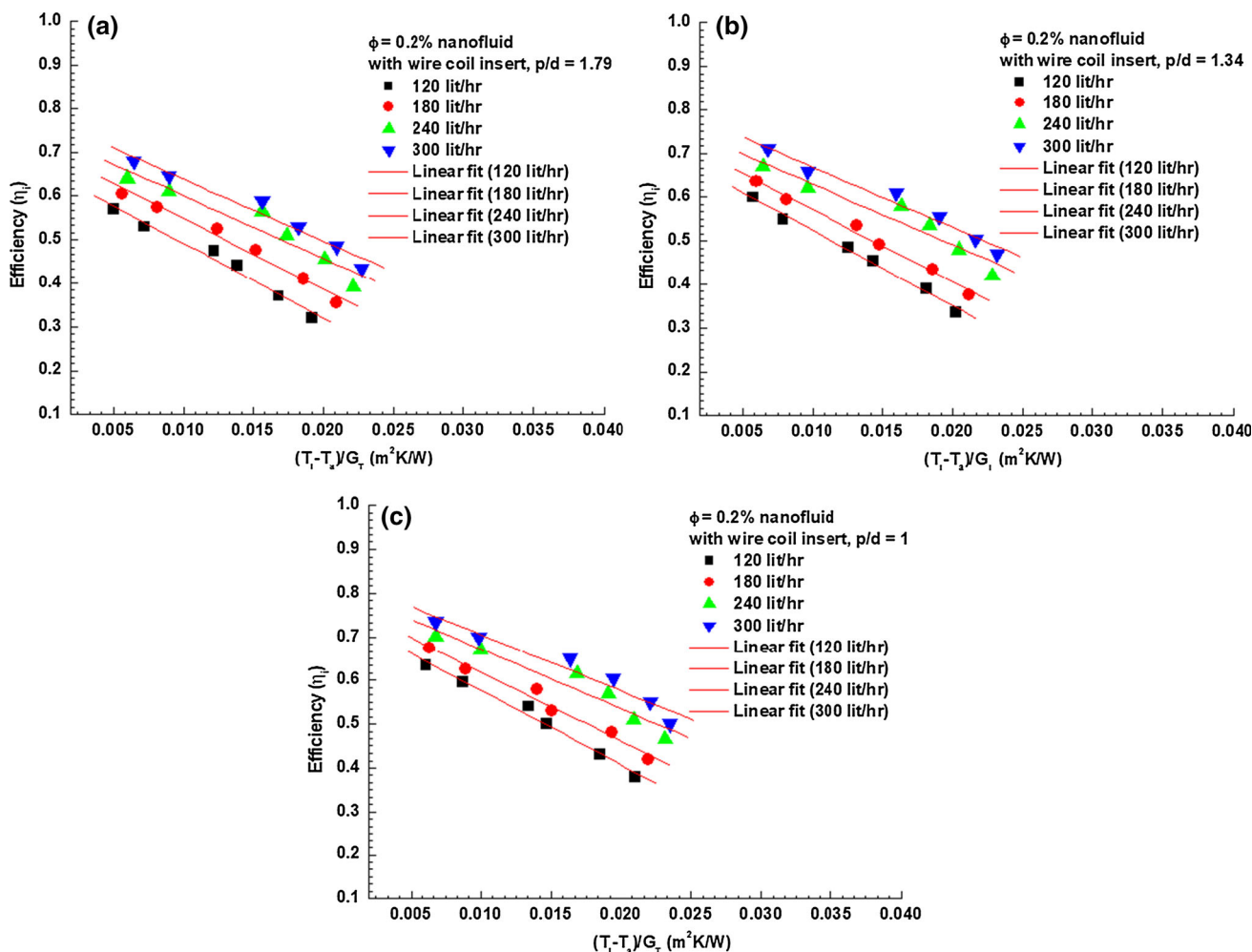**Fig. 9** Thermal efficiency of the collector with $\phi = 0.2\%$ nanofluid and different wire coil inserts at different flow rates: **a** $p/d = 1.79$, **b** $p/d = 1.34$, **c** $p/d = 1$

3.3.2 Plain Collector for Nanofluids and Wire Coil Configurations

The decreased weight calculations were further performed for water and nanofluids with the addition of wire coil configurations. The water with coiled wire pitches of 17.9, 13.4 and 10 mm configurations, the weight of collector decreased to 46.33 kg, in which the glass and copper are 35.21 kg and 11.11 kg, 42.60 kg, in which the glass and copper are 32.42 kg and 10.23 kg, and 41.336 kg, in which the glass and copper are 31.41 kg and 9.91 kg, equivalent to 7.34%, 14.68% and 17.34%, respectively, as compared to water collector weight. To manufacture 100 units of the collector with coiled wire pitches of 17.9, 13.4 and 10 mm configurations, the decreased collector weight is 367 kg, 734 kg and 867 kg, respectively.

When the collector with 0.1% nanofluid and coiled wire pitches of 17.9, 13.4 and 10 mm configurations, the decreased weight is 41.33 kg, in which the glass and copper are 31.41 kg and 9.91 kg, 39.55 kg, in which the glass and copper are

30.05 kg and 9.49 kg 37.83 kg, in which the glass and copper are 28.75 kg and 9.07 kg, which is equal to 17.34%, 20.9% and 24.34% compared to water collector. To make 100 units of the collector with coiled wire pitches of 17.9, 13.4 and 10 mm configurations, the decreased collector weight is 867 kg, 1045 kg and 1217 kg, respectively.

Moreover, the collector with 0.2% nanofluid and coiled wire pitches of 17.9, 13.4 and 10 mm configurations, the collector weight is decreased to 38.33 kg (whereas the glass and copper are 29.51 kg and 9.31 kg), 37.16 kg (in which the glass and copper are 28.24 kg and 8.91 kg) and 36 kg (in which the glass and copper are 27.36 kg and 8.64 kg), which confirms 22.34%, 25.68% and 28%, respectively, as in contrast to water collector. For the production of 100 units of such solar collector with coiled wire pitches of 17.9, 13.4 and 10 mm configurations, the decreased collector weight is 1117 kg, 1284 kg and 1400 kg, respectively.

Meanwhile, the collector with 0.3% nanofluid and coiled wire pitches of 17.9, 13.4 and 10 mm configurations, the

Table 10 The heat removal factor and absorbed energy parameter values of 0.2% and 0.3% nanofluids with various wire coil inserts and flow rates

Wire coil inserts type	Flow rate (L/h)	$\phi = 0.2\%$			$\phi = 0.3\%$		
		$F_R U_L$	$F_R \tau\alpha$	R^2	$F_R U_L$	$F_R \tau\alpha$	R^2
$p/d = 1.79$	120	− 17.14	0.663	0.988	− 16.24	0.701	0.982
	180	− 16.11	0.708	0.970	− 15.76	0.743	0.984
	240	− 14.34	0.744	0.954	− 15.10	0.788	0.969
	300	− 14.17	0.780	0.980	− 14.81	0.832	0.974
$p/d = 1.34$	120	− 17.37	0.697	0.996	− 16.73	0.723	0.995
	180	− 16.58	0.737	0.994	− 14.12	0.749	0.982
	240	− 13.86	0.768	0.960	− 12.84	0.779	0.972
	300	− 13.77	0.806	0.985	− 13.41	0.845	0.978
$p/d = 1$	120	− 17.01	0.747	0.993	− 16.16	0.773	0.990
	180	− 15.66	0.775	0.989	− 14.86	0.806	0.988
	240	− 13.69	0.809	0.964	− 13.33	0.836	0.990
	300	− 12.89	0.834	0.971	− 12.35	0.871	0.970
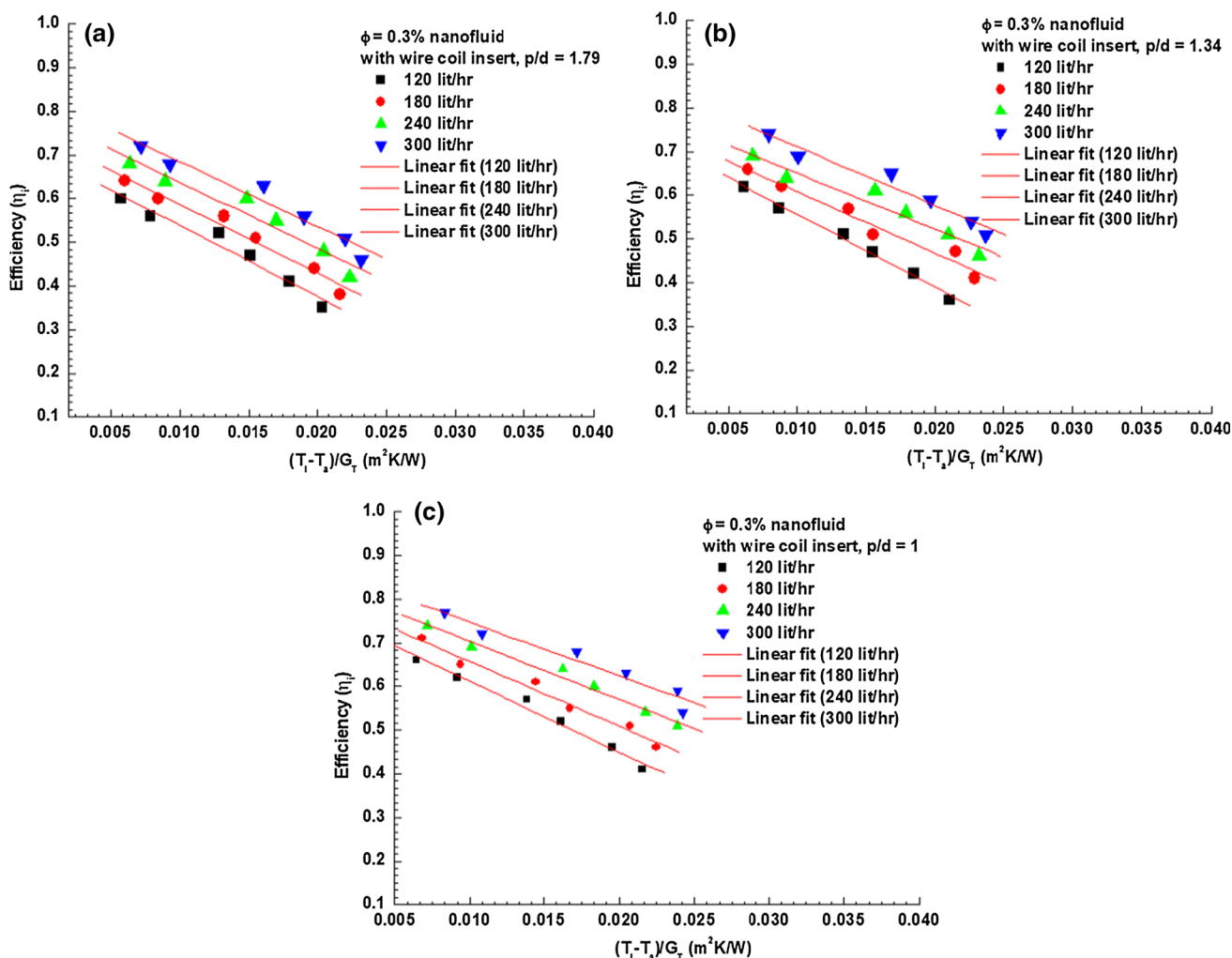
Fig. 10 Thermal efficiency of the collector with $\phi = 0.3\%$ nanofluid and different wire coil inserts at different flow rates: **a** $p/d = 1.79$, **b** $p/d = 1.34$, **c** $p/d = 1$

Fig. 11 Reduced collector area of water and nanofluids with different wire coil inserts
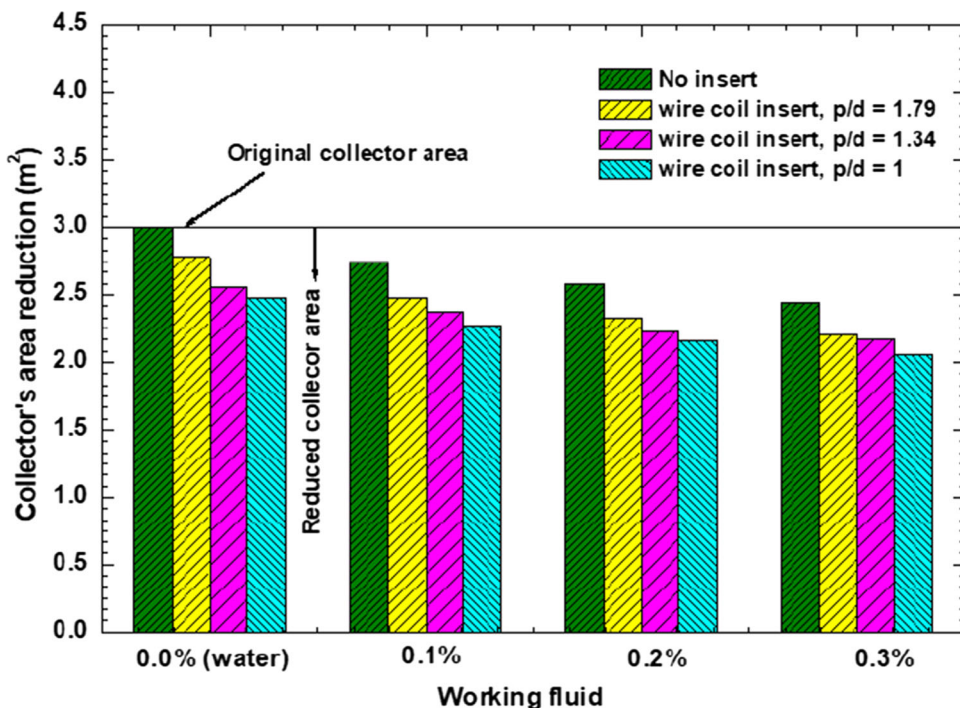
decreased weight of the collector is 36.66 kg (in which the glass and copper are 27.86 kg and 8.67 kg), 36.16 kg (in which the glass and copper are 27.48 kg and 8.67 kg) and 34.33 kg (in which the glass and copper are 26.07 kg and 8.23 kg), which confirms 26.68%, 27.68% and 31.34%, respectively, as compared to water collector. For producing 100 units of the collector with coiled wire pitches of 17.9, 13.4 and 10 mm configurations, the decreased weight is 1334 kg, 1384 kg and 1567 kg, respectively.

3.4 Cost of the Collector

3.4.1 Plain Collector for Nanofluids

The collector cost considering all the components is 223.88$. Utilizing particle loadings of 0.1%, 0.2% and 0.3% particle loadings of nanofluid, the collector cost decreased to 204.47$, 192.53$ and 182.08$, which confirms 8.66%, 14.02% and 18.67%, respectively. To make 100 solar collectors the cost decreased to 1941$ ($\phi = 0.1\%$), 3135$ ($\phi = 0.2\%$) and 4108$ ($\phi = 0.3\%$), respectively.

3.4.2 Plain Collector for Nanofluids and Wire Coil Configurations

Moreover, the efficiency is improved by using wire coil configurations in the collector. This enhanced efficiency is additionally used for collector cost reduction analysis. For the water collector with coiled wire pitches of 17.9, 13.4 and 10 mm configurations, the collector cost is reduced to 207.46$, 191.04$ and 185.07$, which confirms 7.33%, 14.36% and 17.33%, respectively, as compared to water collector. For producing 100 units of the solar collector, the cost is decreased to 1642$, 3284$ and 3881$, respectively.

The cost of the collector for 0.1% nanofluid with coiled wire pitches of 17.9, 13.4 and 10 mm configurations, is reduced to 185.07$, 176.86$, 169.40$, which confirms 17.33%, 21% and 24.24%, respectively, as compared to water collector. For the production of 100 solar collectors, the cost is reduced to 3881$, 4702$ and 5448$, respectively.

When using 0.2% of nanofluid in plain collector with coiled wire pitches of 17.9, 13.4 and 10 mm configurations, the collector cost is reduced to 173.88$, 166.41$ and 161.19$, which confirms 22.33%, 25.67% and 28%, respectively, compared to water collector. For manufacturing 100 solar collectors, the cost is reduced to 5000$, 5747$ and 6269$, respectively.

With the use of nanofluid with 0.3% particle loading in plain collector with coiled wire pitches of 17.9, 13.4 and 10 mm configurations, the collector cost is reduced to 164.17$, 161.93$ and 153.73$, which confirms 26.67%, 27.71% and 31.33%, respectively, as in contrast to water collector. For the production of 100 units of solar collector, the cost is lessened to 5971$, 6195$ and 7015$, respectively. The decreased collector cost with the effect of percentage is provided in Table 11, and the same collector cost with coiled wire pitches of 17.9, 13.4 and 10 mm configurations is shown in Fig. 12.

Table 11 The cost reduction of the collector with nanofluids and wire coil inserts (USD)

Fluid	Reduced cost of the collector (USD)							
	Plan tube (no insert)		$p/d = 1.79$		$p/d = 1.34$		$p/d = 1$	
	Cost (USD)	Reduction (%)	Cost (USD)	Reduction (%)	Cost (USD)	Reduction (%)	Cost (USD)	Reduction (%)
Water	223.88	–	207.46	7.33	191.04	14.36	185.07	17.33
0.1%	204.47	8.66%	185.07	17.33	176.86	21	169.40	24.24
0.2%	192.53	14%	173.88	22.33	166.41	25.67	161.19	28
0.3%	182.08	18.67%	164.17	26.67	161.93	27.71	153.73	31.33

Fig. 12 Reduced collector cost of water and nanofluids with different wire coil inserts
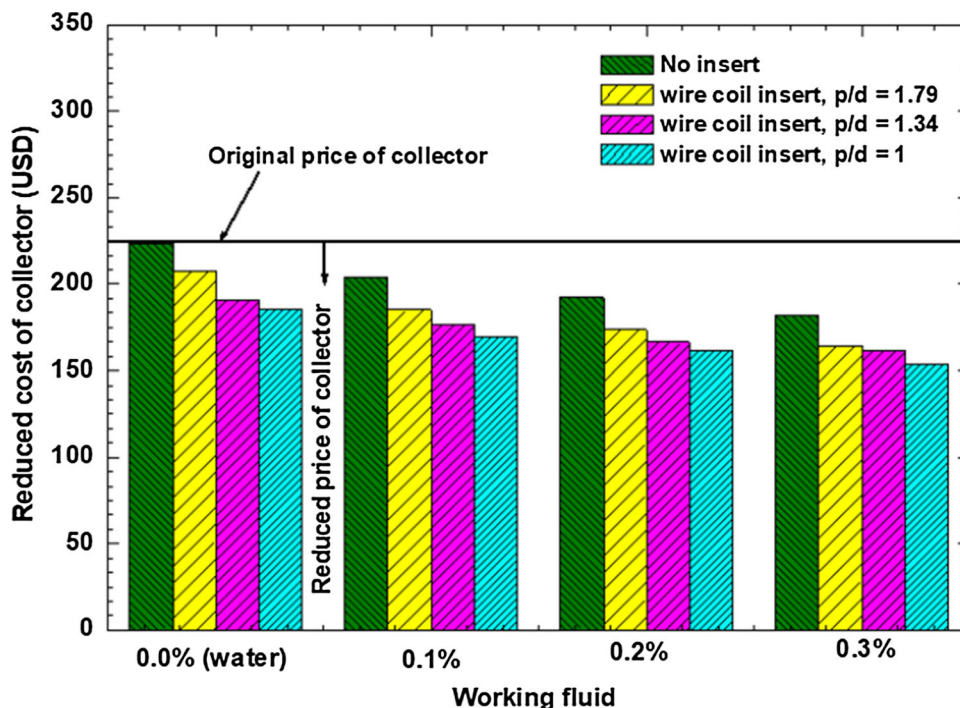
3.5 Energy Reduction of Collector

3.5.1 Plain Collector for Nanofluids

Each utilized material has its own embodied energy. Since glass and copper are the primary material considered for collectors. Hence, the embodied energy of glass and copper is considered for the calculations. In general, the embodied energy of the copper and glass is 70.6 MJ/kg and 15.9 MJ/kg [39], respectively. Since the weight of the collector is 50 kg, based on the embodied energy, it is found that the represented energy including glass and copper material for the collector with water is 1451.4 MJ, which is decreased to 1325.65 MJ ($\phi = 0.1\%$), 1248.20 MJ ($\phi = 0.2\%$) and 1144.36 MJ ($\phi = 0.3\%$), respectively.

3.5.2 Plain Collector for Nanofluids and Wire Coil Configurations

The water collector with coiled wire pitches of 17.9, 13.4 and 10 mm configurations, the embodied energy decreased to 1344.19 MJ, 1241.70 MJ and 1199.05 MJ compared to the plain collector with water.

With $\phi = 0.1\%$ vol. concentration of collector with coiled wire pitches of 17.9, 13.4 and 10 mm configurations, the embodied energy decreased to 1149.05 MJ, 1147.78 MJ and 1097.46 MJ compared to plain collector with water. However, with $\phi = 0.2\%$ vol. concentration of collector with coiled wire pitches of 17.9, 13.4 and 10 mm configurations, the embodied energy decreased to 1126.43 MJ, 1078.05 MJ and 1047.12 MJ compared to the plain collector with water. Meanwhile, with $\phi = 0.3\%$ vol. concentration of collector with coiled wire pitches of 17.9, 13.4 and 10 mm configurations, the embodied energy is reduced to 1063.54 MJ, 1049.03 MJ and 1022.86 MJ compared to plain collector

Fig. 13 Reduced embodied energy of the collector material with the use of water and nanofluids in collector with various wire coil inserts
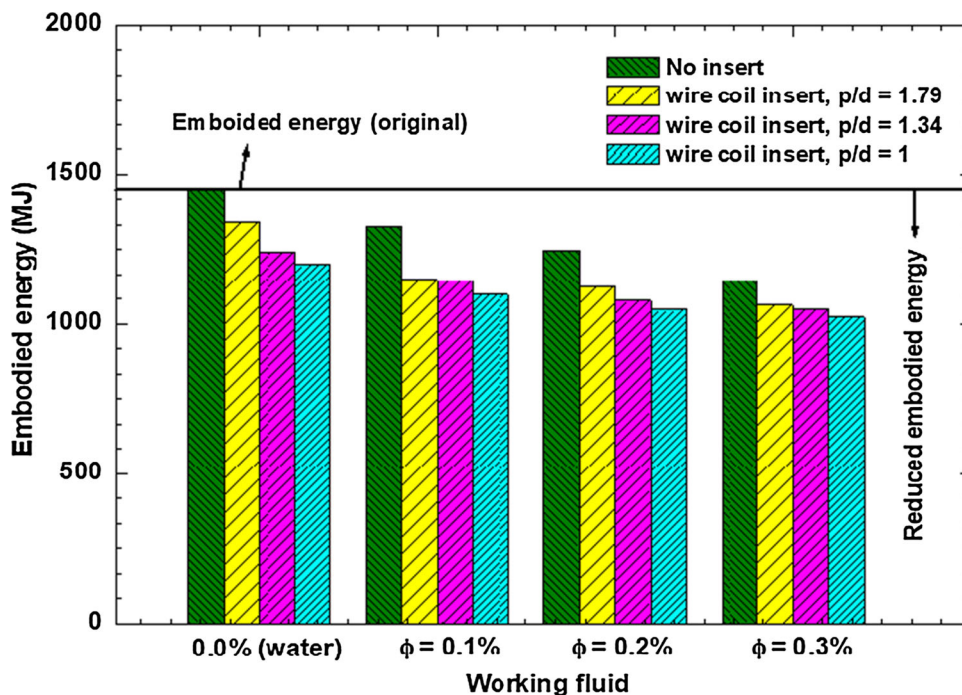
with water. The reduced embodied energy of the collector is presented in Fig. 13.

3.6 Emissions Analysis

3.6.1 Nanofluids in Plain Collector

The collector manufacturing using Al_2O_3/water nanofluids results in a decrease in CO_2 emissions. These emissions are further reduced with an increase in particle loadings. The CO_2 emissions of water collector are 880.9 kg, which is decreased to 804.57 kg (76.32 kg), 757.57 kg (123.32 kg) and 694.54 kg (186.35 kg) of 0.1%, 0.2% and 0.3% of volume concentrations for nanofluids. The component of other emissions, such as nitrogen oxides (NO_x) and sulfur oxides (SO_x), is much smaller.

3.6.2 Plain Collector for Nanofluids and Wire Coil Configurations

The collectors with Al_2O_3 nanofluids and inserted coiled wires result in further reduction of CO_2 emissions. The CO_2 emission of the water collector is 880.9 kg, which is decreased to 815.83 kg, 753.62 kg and 727.74 kg for water with coiled wire pitches of 17.9, 13.4 and 10 mm configurations, respectively.

The CO_2 emissions of $\phi = 0.1\%$ nanofluid are 804.57 kg, which is reduced to 697.39 kg, 696.62 kg and 666.08 kg for $\phi = 0.1\%$ nanofluid with coiled wire pitches of 17.9, 13.4 and 10 mm configurations, respectively. The CO_2 emissions

of $\phi = 0.2\%$ nanofluid are 757.57 kg, which is reduced to 683.69 kg, 654.42 kg and 635.52 kg for $\phi = 0.2\%$ nanofluid with coiled wire pitches of 17.9, 13.4 and 10 mm configurations, respectively.

The CO_2 emissions of $\phi = 0.3\%$ nanofluid are 694.54 kg, which is reduced to 645.49 kg, 636.68 kg and 620.80 kg for $\phi = 0.3\%$ nanofluid with coiled wire pitches of 17.9, 13.4 and 10 mm configurations, respectively. The other components of emissions like sulfur oxides (SO_x) and nitrogen oxides (NO_x) are very small. Table 12 shows the embodied energy emissions from different particle loadings and inserts. Limited studies have been reported showing the use of nanofluids in solar collectors, and their impact on CO_2 emissions, such as those presented by Faizal et al. [40] and Stalin et al. [41] for various kinds of nanofluids.

3.7 Plain Collector Nanofluid Nusselt Number

The heat absorbed by the fluid is evaluated from the below equations.

Rate of heat, $\dot{Q} = \dot{m} \times c_p \times (T_o - T_i)$ (17)

The below-mentioned Newton's equation is considered to estimate the coefficient of heat transfer.

Coefficient of heat transfer, $h_{exp} = \dfrac{\dot{Q}}{A\,(T_s - T_b)}$ (18)

Table 12 The present study of embodied energy and energy saving with the use of Al_2O_3 nanofluid compared with the previous studies

Fluid	Insert type	Embodied energy (MJ)	Emissions carbon dioxide (CO_2)	Sulfur oxides (SO_x)	Nitrogen oxides (NO_x)
Water	Plain tube	1451.4	880.9	0.4492	0.768
	$p/d = 1.79$	1344.19	815.83	0.4152	0.7112
	$p/d = 1.34$	1241.7	753.62	0.3844	0.6570
	$p/d = 1$	1199.05	727.74	0.3703	0.6344
$\phi = 0.1\%$	Plain tube	1325.65	804.57	0.4102	0.7014
	$p/d = 1.79$	1149.05	697.39	0.3554	0.6080
	$p/d = 1.34$	1147.78	696.62	0.3550	0.6073
	$p/d = 1$	1097.46	666.08	0.3395	0.5807
$\phi = 0.2\%$	Plain tube	1248.2	757.57	0.3861	0.6604
	$p/d = 1.79$	1126.48	683.69	0.3484	0.5960
	$p/d = 1.34$	1078.25	654.42	0.3335	0.5705
	$p/d = 1$	1047.12	635.52	0.3239	0.5540
$\phi = 0.3\%$	Plain tube	1144.36	694.54	0.3540	0.6055
	$p/d = 1.79$	1063.54	645.49	0.3290	0.5627
	$p/d = 1.34$	1049.03	636.68	0.3245	0.5550
	$p/d = 1$	1022.86	620.80	0.3164	0.5412
Stalin et al. [41] for CeO_2/water nanofluid, $\phi = 0.1\%$	Plain tube	887.2	538.53	0.275	0.4701
Faizal et al. [42] for SiO_2/water nanofluid	Plain tube	928	563.30	0.28768	0.49184

xThe terms in Eq. (18) are area $A = \pi DL$, surface temperature $\left(T_s = \frac{T_1+T_2+T_3}{3}\right)$ and bulk mean temperature $\left(T_b = \frac{T_i+T_o}{2}\right)$.

The Nusselt number, $\mathrm{Nu_{exp}} = \dfrac{h_{exp} \times D}{k}$ (19)

The Prandtl number, $\mathrm{Pr} = \dfrac{\mu c_p}{k}$ (20)

The equation for single-phase fluid from Gnielinski [42] was used for the comparison of water data

$$\mathrm{Nu} = \frac{\left(\frac{f}{2}\right)(\mathrm{Re} - 1000)\mathrm{Pr}}{1 + 12.7\left(\frac{f}{2}\right)^{0.5}\left(\mathrm{Pr}^{2/3} - 1\right)} \quad (21)$$

$f = (1.58\ln\mathrm{Re} - 3.82)^{-2}$

$2300 < \mathrm{Re} < 5 \times 10^6; 0.5 < \mathrm{Pr} < 2000$

The water Nusselt number (Eq. 19) from experiments is provided in Fig. 14, in comparison with Gnielinski [42] data, and a maximum of $\pm 2.5\%$ deviation between them was noted. The nanofluids Nusselt number (Eq. 19) from experiments is shown in Fig. 15 in comparison with water. The nanofluids' Nusselt number increased employing added particle loadings and Reynolds numbers. Because of the enhanced thermal properties of the nanofluids, Brownian motion of the nanoparticles, the Nusselt number enhanced. The Nusselt number augmented to 5.57% (Re = 5000) and 14.42% (Re = 13,500) for 0.1% nanofluid, 6.78% x(Re = 5000) and 18.33% (Re = 13,500) for 0.2% nanofluid and 9.74% (Re = 5000) and 23.22% (Re = 13,500) for 0.3% nanofluid in comparison with water.

### 3.8 Plain Collector Water Nusselt Number and Wire Coil Configurations

The collector is analyzed experimentally with the coiled wire pitches of 17.9, 13.4 and 10 mm configurations added to tubes with water flowing in them, and the experimental Nusselt number (Eq. 19) is shown in Fig. 16, along with Garcia et al. [22] data for validation purposes. Garcia et al. [22] equation is presented below:

$$\mathrm{Nu} = 0.303\,\mathrm{Re}^{0.72}\mathrm{Pr}^{0.37}\left(\frac{p}{d}\right)^{-0.377}\left(\frac{e}{d}\right)^{0.12} \quad (22)$$

$1500 < \mathrm{Re} < 60,000; 1.17 < \dfrac{p}{d} < 2.68; \mathrm{Pr} = 2.8$

It is noted from thexs figure that at the same Reynolds number, the Nusselt number data for Garcia et al. [22] present higher values than those of the present data. This discrepancy

Fig. 14 Comparison of the experimental Nusselt number versus Reynolds number for water against the data of Gnielinski [42]
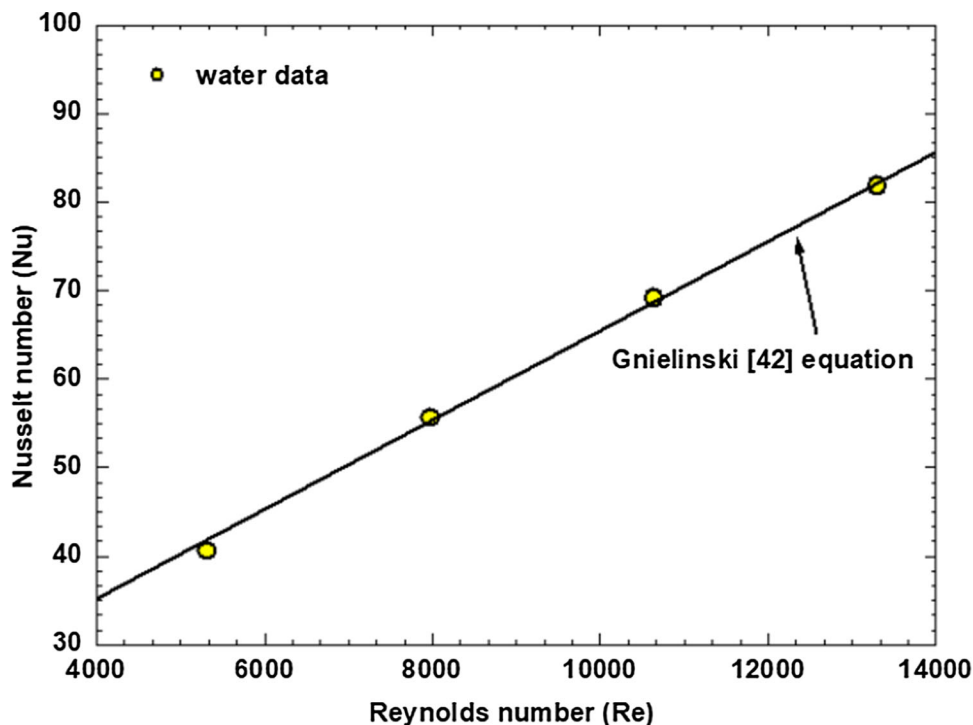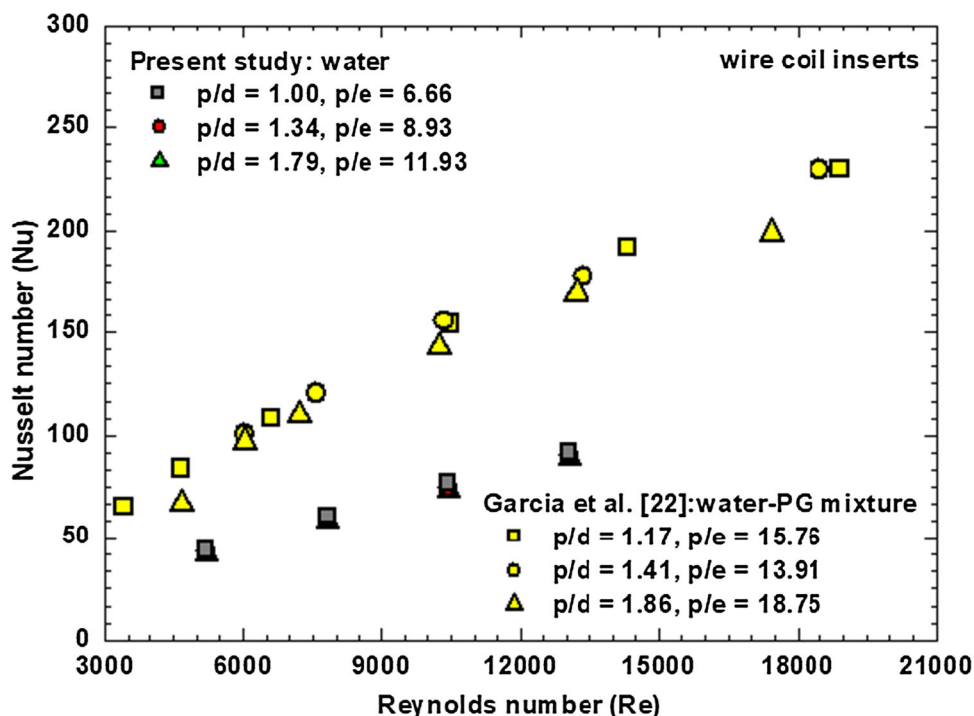

Fig. 15 Experimental Nusselt number versus Reynolds number of nanofluids at different volume concentrations
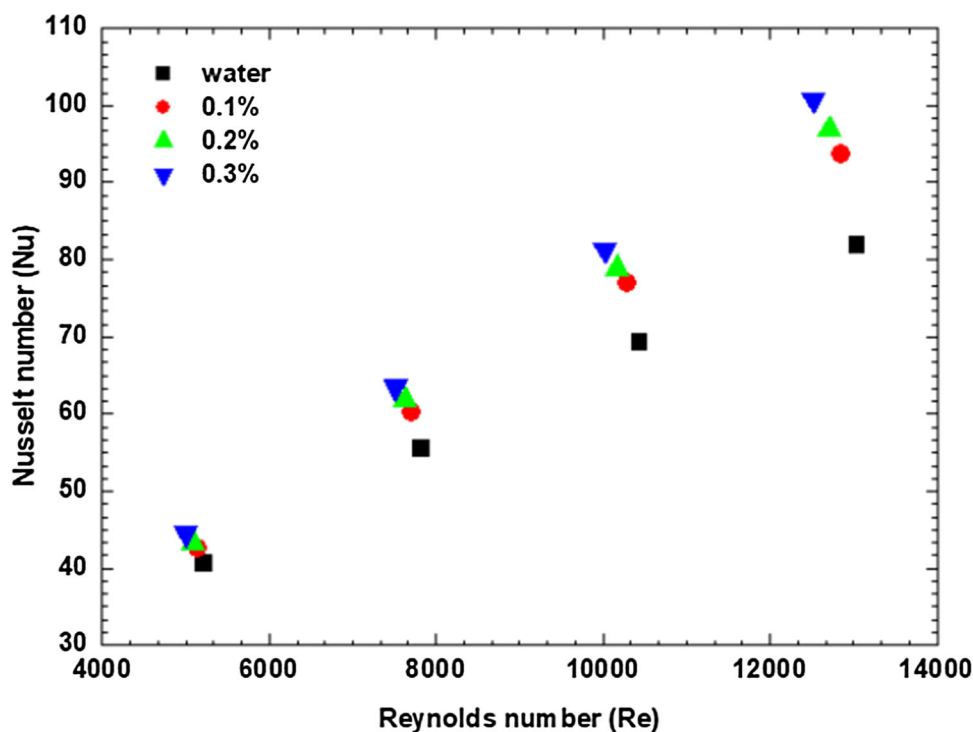

may be attributed to the difference in the experimental setups and of the operating conditions. For comparison purposes the water data with no inserts show that the Nusselt number enhancement of coiled wire pitch of 17.9 mm is 3.82% (Re = 5000) and 8.13% (Re = 13,500), for coiled wire pitch of 13.4 mm is 6.07% (Re = 5000) and 10.30% (Re = 13,500) and for coiled wire pitch of 10 mm is 7.28% (Re = 5000) and 11.93% (Re = 13,500), respectively.

Fig. 16 Comparison of the experimental Nusselt number versus Reynolds number of water with wire coil inserts data against the data of Garcia et al. [22]

Fig. 17 Experimental Nusselt number versus Reynolds number of water and nanofluids flow in the flat-plate solar collector with wire coil inserts
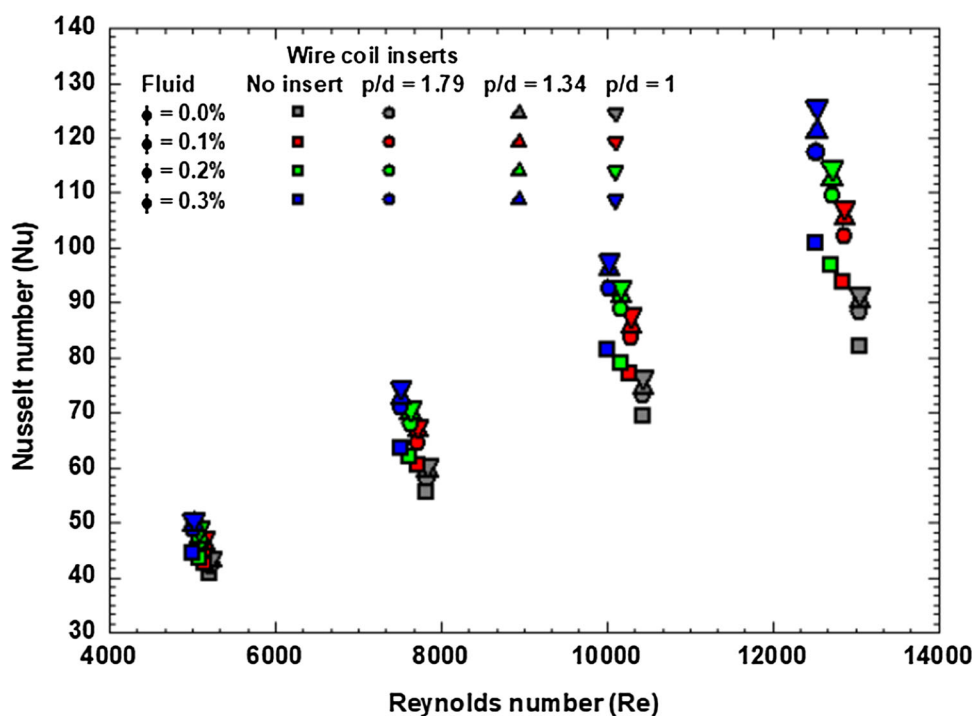
3.9 Plain Collector Nanofluid Nusselt Number and Wire Coil Configurations

Similar experiments were repeated using the Al_2O_3 nanofluids as the working fluid, where the influence of coiled wire pitches of 17.9, 13.4 and 10 mm configurations is inserted in the flat-plate collector; Eq. (18) was estimated for the experimental Nusselt number, and the data are displayed in Fig. 17. For comparison purposes, the data of the nanofluids with 0.1% particle loading and with no inserts are compared, where the Nusselt number enhancement for coiled wire pitches of 17.9, 13.4 and 10 mm configurations is 5.16% (Re = 5000) and 9.10% (Re = 13,500), 8.22% (Re = 5000)

and 12.66% (Re = 13,500) and 10.56% (Re = 5000) and 14.68% (Re = 13,500), respectively.

For further comparison using nanofluids with 0.2% particle loading and with no inserts are evaluated where the Nusselt number enhancement for coiled wire pitch of 17.9 mm is 7.39% (Re = 5000) and 13.24% (Re = 13,500), for coiled wire pitch of 13.4 mm is 9.70% (Re = 5000) and 16.36% (Re = 13,500) and for coiled wire pitch of 10 mm is 12.93% (Re = 5000) and 18.41% (Re = 13,500), respectively.

Furthermore data of nanofluids with 0.3% particle loadings and with no inserts are compared where the Nusselt number enhancement for coiled wire pitch of 17.9 mm is 9.39% (Re = 5000) and 16.49% (Re = 13,500), for coiled wire pitch of 13.4 mm is 11.51% (Re = 5000) and 20.25% (Re = 13,500) and for coiled wire pitch of 10 mm is 13.75% (Re = 5000) and 24.62% (Re = 13,500), respectively.

Comparison using the water data with no inserts indicates that the Nusselt number enhancement for nanofluids with 0.1%, 0.2% and 0.3% particle loadings and with coiled wire pitch of 10 mm is 16.15% (Re = 5000) and 31.22% (Re = 13,500), 20.59% (Re = 5000) and 40.12% (Re = 13,500) and 24.83% (Re = 5000) and 53.56% (Re = 13,500), respectively. The main cause for the heat transfer augmentation with coiled wire configurations increases further with mixing, generating turbulence. The heat transfer enhancement is higher for a coiled wire pitch of 10 mm than that for 17.9 mm and 13.4 due to the decrease in the flow area. Nanofluid with 0.3% particle loading and coiled wire pitch of 10 mm as well as the same flow rate, shows higher heat transfer enhancement compared to the arrangements tested, as a result of a combination of improved thermal properties, enhanced fluid mixing, turbulence generation and motion of nanoparticles (Brownian).

To better understand the data trend of nanofluids as the flat-plate collector working fluid, the present information for 0.3% nanofluid with coiled wire pitches of 17.9, 13.4 and 10 mm configurations is reported in Fig. 18, along with Akhavan-Behabadi et al. [43] data for validation. Akhavan-Behabadi et al. [43] conducted their experiments for MWCNT/water nanofluids flowing in a horizontal tube with a pitch to diameter value equal to 1.70 and 2.27, and they proposed a regression equation, which is given as:

$$Nu = 0.1763(Re)^{0.6837}Pr^{0.0442}(1 + \phi)^{0.6877}\left(1 + \frac{p}{d}\right)^{0.0761} \tag{23}$$

$$10,000 < Re < 20,000; 4.5 < Pr < 6.5; 1.70$$
$$< p/d < 2.83; 0.113 < e/d < 0.170$$

From Fig. 18, the values from Akhavan-Behabadi et al. [43] for MWCNT nanofluids have slightly higher values than that of the present Al$_2$O$_3$/water nanofluids, which

may be due to enhanced nanofluid thermal conductivity (MWCNT/water) in comparison with Al$_2$O$_3$ nanofluids.

The present experimental Nusselt number of Al$_2$O$_3$ nanofluid and with coiled wire inserts values (48 data points) was fitted into a regression equation in the similar lines of Garcia et al. [22] and Akhavan-Behabadi et al. [43] with deviations of 4.203% (mean) and 5.328% (standard), and the equation is presented below.

$$Nu_{Reg} = 0.02332Re^{0.8}Pr^{0.4}(1 + \phi)^{0.6435}\left(1 + \frac{p}{d}\right)^{0.07210} \tag{24}$$

$$5000 < Re < 13,500; 4.4 < Pr < 5.71; 0$$
$$< p/d < 1.79; 0 < \phi < 0.3\%$$

The measured data and data from Eq. (24) are indicated in Fig. 19.

3.9.1 Plain Collector Nanofluid Friction Factor

The benchmark of friction factor measurements was performed for water, and later it is extended to nanofluids. The Fanning friction from Eq. (25) was evaluated for water and presented in Fig. 20, in comparison with Blasius [44] values for validation.

$$f_{Exp} = \frac{(\Delta P)}{\left(\frac{L}{D}\right)\left(\frac{\rho v^2}{2}\right)} \tag{25}$$

The Blasius [44] for single-phase fluid is given by Eq. (26), namely:

$$f = 0.3164Re^{-0.25} \tag{26}$$

The present data show ±2.5% deviation in comparison with the Blasius relation. Consequently, the friction factor experiments were carried out with various particle loadings and flow rates. As for the water, Eq. (25) was considered for friction factor evaluations, and the values are shown in Fig. 21. It can be noted that with the increase of particle volume concentration, the friction factor also increases; however, the increase of Reynolds number yields a decrease in the friction factor. The increase of friction factor, when nanofluids are used, is caused by the increase of frictional resistance between the fluid layers, as compared to pure water. The penalty in coefficient of friction for 0.1%, 0.2% and 0.3% nanofluids when compared to the water data, is 4.9% (Re = 5000) and 9.8% (Re = 13,500), 5.91% (Re = 5000) and 13.38% (Re = 13,500) and 7.08% (Re = 5000) and 16.94% (Re = 13,500), respectively.

Fig. 18 Comparison of the experimental Nusselt number versus Reynolds number of nanofluid (0.3%) in a solar flat-plate collector with wire coil inserts against the data of Akhavan-Behabadi et al. [38] for MWCNT/water nanofluids
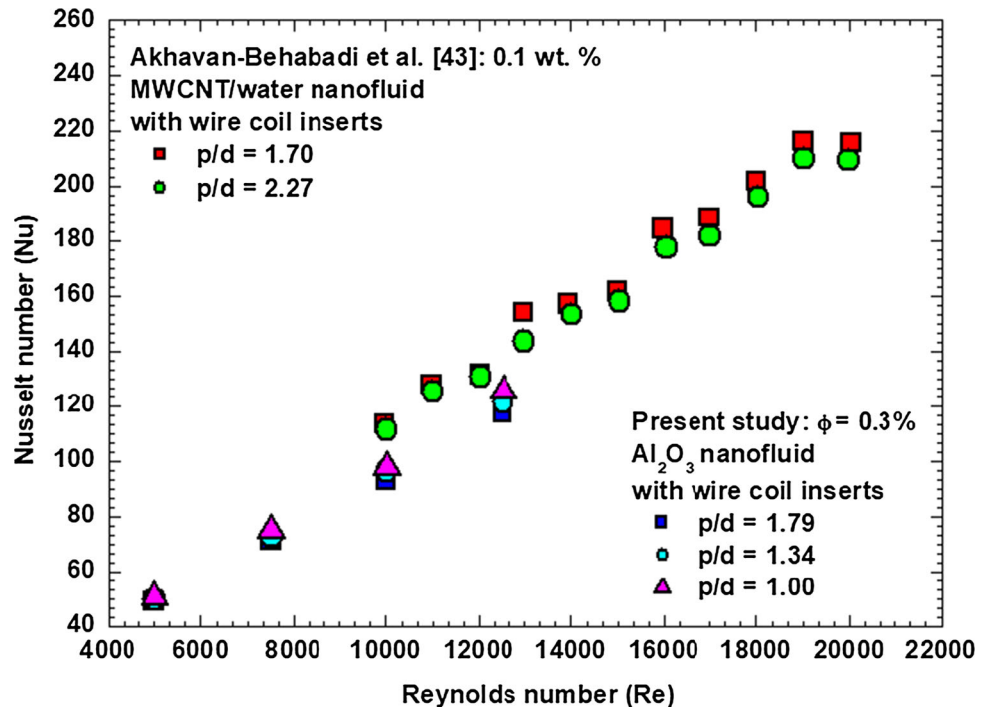
Fig. 19 The experimental data compared with the proposed Nusselt number correlation
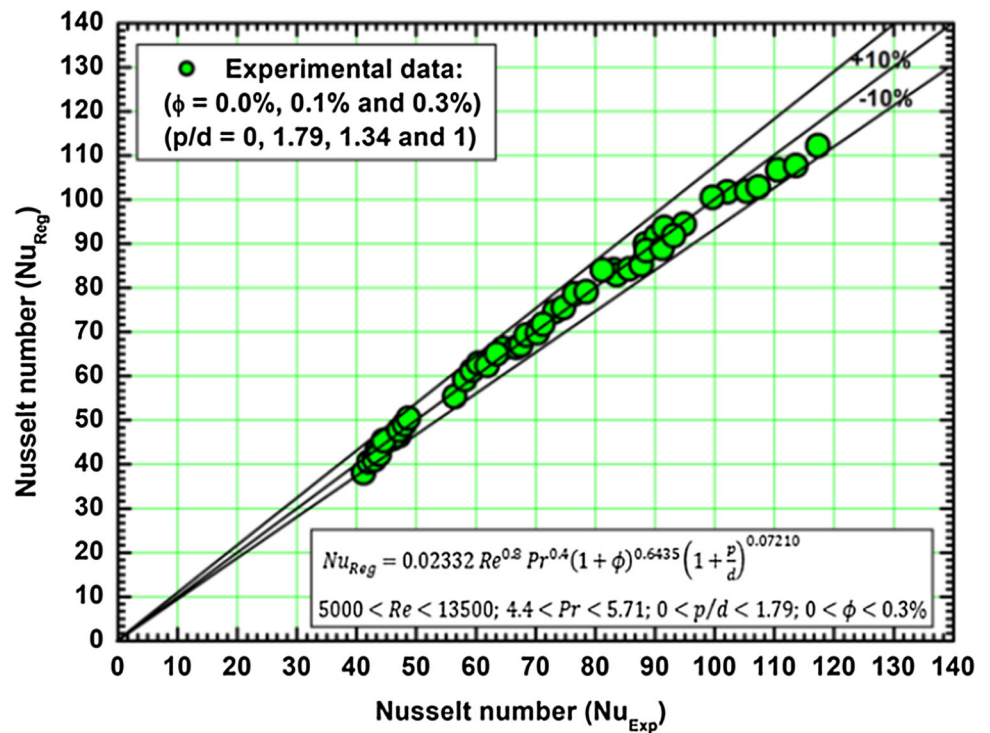

3.9.2 Plain Collector Water Friction Factor and Wire Coil Configurations

The influence of coiled wire pitches of 17.9, 13.4 and 10 mm configurations added in water/nanofluids and its friction factor was examined. First, the experiments were conducted using water with coiled wire pitches of 17.9, 13.4 and 10 mm

configurations, Eq. (25) was considered for friction factor evaluations, and the data are displayed in Fig. 22 in comparison with Garcia et al. [22] data for validation. Garcia et al. [22] proposed a regression equation, which is given as:

$$f = 5.76\text{Re}^{-0.217}\left(\frac{p}{d}\right)^{-1.21}\left(\frac{e}{d}\right)^{0.95} \tag{27}$$

Fig. 20 Comparison of the experimental friction factor versus Reynolds number of water in the flat-plate solar collector against the data of Blasius [44]
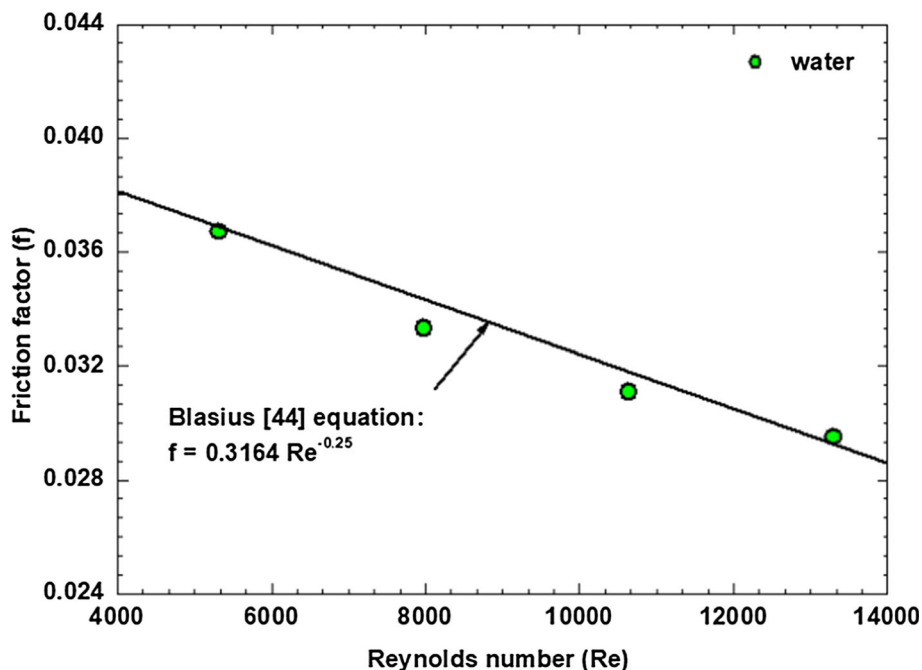
Fig. 21 Experimental friction factor versus Reynolds number of nanofluids flow in the solar flat-plate collector at different volume concentrations
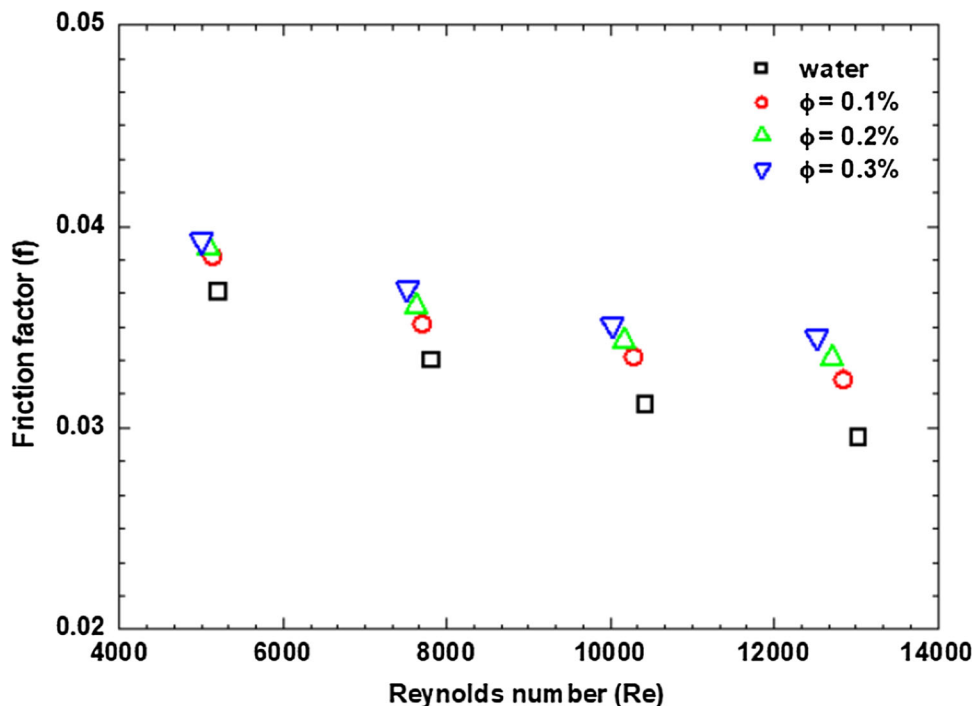

$$2000 < \mathrm{Re} < 30,000; 1.17 < \frac{p}{d} < 2.68; \mathrm{Pr} = 2.8$$

Close observation of Fig. 22 shows that, for the same values of the Reynolds number, the friction factor of Garcia et al. [22] demonstrates higher values than that of the present data. The apparent discrepancy may be explained based on the experimental setups and also the operating conditions being different. The penalty in friction factor of coiled wire pitches of 17.9, 13.4 and 10 mm configurations, when compared to water data, is 3.81% (Re = 5000) and 5.76% (Re = 13,500), 6.53% (Re = 5000) and 8.13% (Re = 13,500) and 8.71% (Re = 5000) and 11.18% (Re = 13,500), respectively.

Fig. 22 Comparison of the experimental friction factor versus Reynolds number of water with wire coil inserts data against the data of Garcia et al. [22]
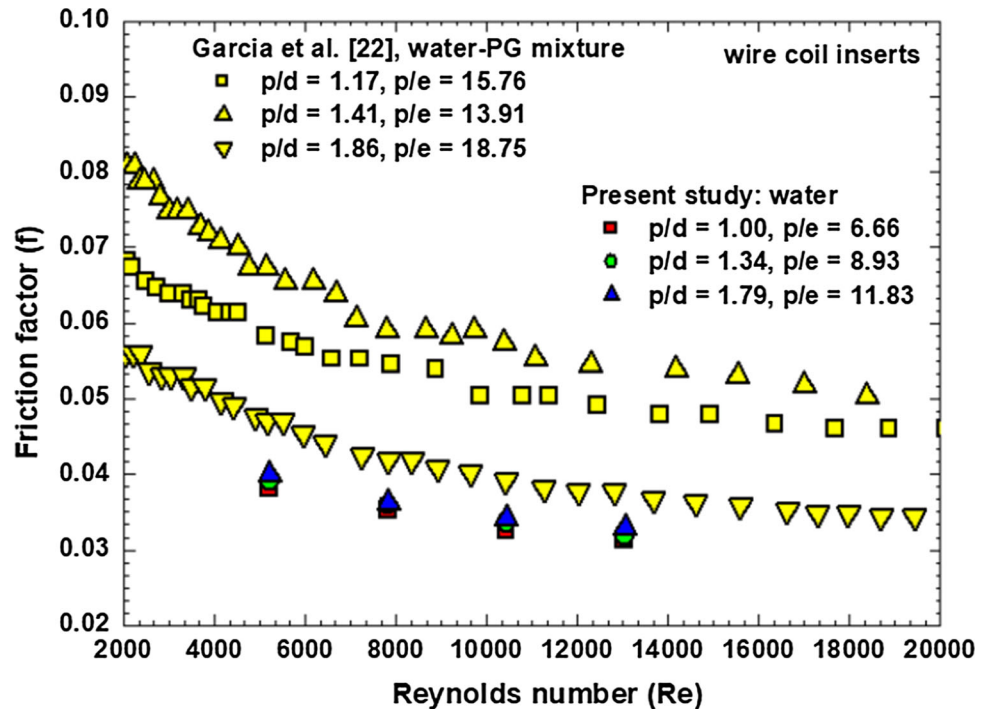
Fig. 23 Experimental friction factor versus Reynolds number of water and nanofluids flow in the solar flat-plate collector with wire coil inserts
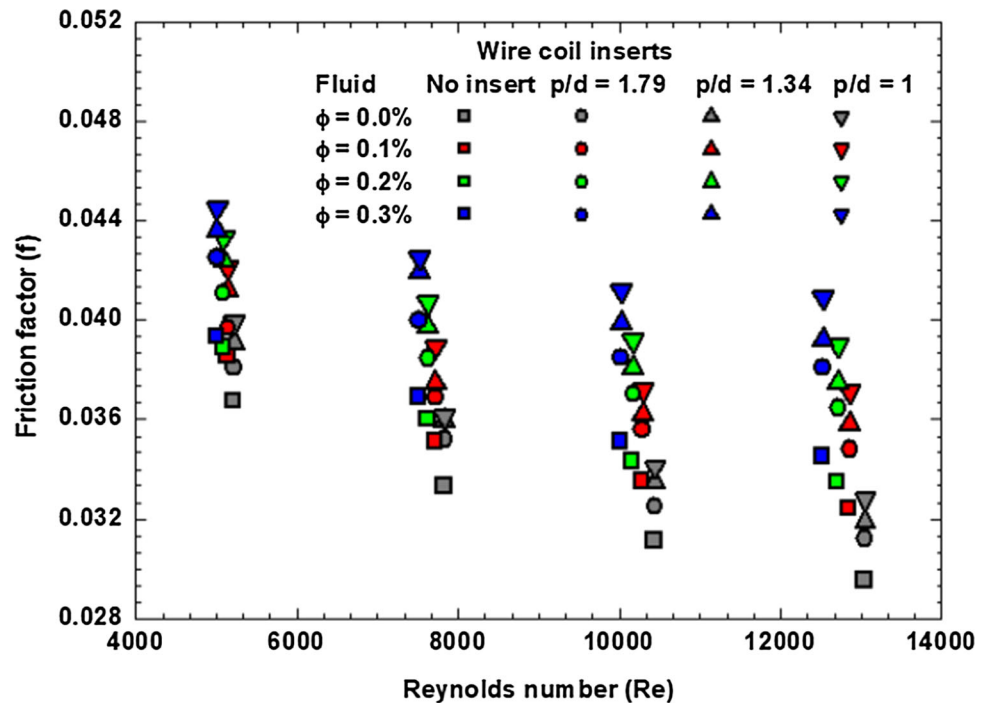
3.9.3 Plain Collector Nanofluid Friction Factor and Wire Coil Configurations

Similar experiments conducted using the Al_2O_3 nanofluids circulate in riser tubes added with coiled wire pitches of 17.9, 13.4 and 10 mm configurations, Eq. (25) was considered for friction factor evaluations, and the values are indicated in Fig. 23.

For the 0.1% nanofluid data, comparison between no inserts and with inserts indicates that the friction factor penalty for coiled wire pitches of 17.9, 13.4 and 10 mm configurations is 3.11% (Re = 5000) and 7.40% (Re = 13,500), 7.01% (Re = 5000) and 10.49% (Re = 13,500) and 9.35% (Re = 5000) and 14.50% (Re = 13,500), respectively. Similarly, comparing the data of nanofluid with 0.2% particle loading without inserts showed a penalty in friction factor

for coiled wire pitches of 17.9, 13.4 and 10 mm configurations is 5.65% (Re = 5000) and 8.90% (Re = 13,500), 8.99% (Re = 5000) and 12.10% (Re = 13,500) and 11.31% (Re = 5000) and 16.59% (Re = 13,500), respectively. Moreover, the nanofluid with 0.3% particle loading in comparison with no inserts data showed a penalty in friction factor for coiled wire pitches of 17.9, 13.4 and 10 mm configurations is 8.14% (Re = 5000) and 10.43% (Re = 13,500), 10.94% (Re = 5000) and 13.62% (Re = 13,500) and 13.23% (Re = 5000) and 18.55% (Re = 13,500), respectively.

It can be noted that for the same value of the Reynolds number, the friction factor penalty for coiled wire pitch of 10 mm is higher than that for coiled wire pitches of 13.4 mm and 17.9 mm. Further comparison using the water data with no inserts as reference yields for the 0.1%, 0.2%, and 0.3% nanofluid with coiled wire pitch of 10 mm, a friction factor penalty of 25.76%, 32.20%, and 38.64% at a Reynolds number of 13,500, respectively.

To better understand the data trend of the friction factor, when nanofluids are in conjunction with the inserts and used in the solar flat-plate collector, the present data for 0.3% nanofluid with coiled wire pitches of 17.9, 13.4, and 10 mm configurations are displayed in Fig. 24, along with Akhavan-Behabadi et al. [43] data for validation. Akhavan-Behabadi et al. [43] conducted the experiments for MWCNT/H$_2$O nanofluids flowing in a horizontal tube with a pitch to diameter ratio of 1.70 and 2.27, and they proposed a regression equation, which is given as:

$$f = 0.7026(\text{Re})^{-0.21}(1+\phi)^{0.44}\left(1+\frac{p}{d}\right)^{0.02}(1+e/d)^{0.79}$$
(28)

$$10000 < \text{Re} < 20,000; 4.5 < \text{Pr} < 6.5; 1.70$$
$$< p/d < 2.83; 0.113 < e/d < 0.170$$

It can be noted from Fig. 24 that the friction factor of Akhavan-Behabadi et al. [43] has slightly higher values than that for present nanofluids data. This difference can be attributed due to the different shapes of the nanoparticles; the Al$_2$O$_3$ spherical particles offer less flow resistance compared to the MWCNT.

The obtained data of Al$_2$O$_3$ nanofluid and addition of coiled wire configurations data are fitted into a regression equation in the similar lines of Garcia et al. [22] and Akhavan-Behabadi et al. [43] and found an AD of 3.88% and SD of 4.96%; the equation is presented below.

$$f_{\text{Reg}} = 0.1324\text{Re}^{-0.1516}(1+\phi)^{0.4291}\left(1+\frac{p}{d}\right)^{0.072}$$
(29)

$$5000 < \text{Re} < 13,500; 4.4 < \text{Pr} < 5.71; 0$$
$$< p/d < 1.79; 0 < \phi < 0.3\%$$

The experimental friction factor and Eq. (29) values are shown in Fig. 25.

3.9.4 Comparison of efficiency

The comparison of the present study with previous literature is shown in Table 13. Zamzamianet al. [16], Sharafeldin and Grof. [46] and Ghaderian et al. [47] also obtained enhanced collector efficiency with the addition of nanofluids in the collector. Sharafeldin et al. [45] and Choudhary et al. [6] obtained 51% and 69.24% efficiencies for the collector employing Cu/water and ZnO/50:50 EG:W nanofluids. In the current study, utilizing 0.3% nanofluid, the efficiency of the collector augmented to 22.64% and further augmented to 45.28% by adding a coiled wire insert pitch of 10 mm. Saleh and Sundar [48] have observed that the collector thermal efficiency increases from 57.15% utilizing water to 69.85% utilizing nanofluid with a concentration of 1.0%. Saleh and Sundar [49] noticed that the collector thermal efficiency is improved to 28.09% at $\phi = 0.3\%$ at 13:00 h daytime and a Re of 1413 over water data.

Zamzamian et al. [16] have conducted experiments for analyzing the collector thermal efficiency with the use of Cu/ethylene glycol nanofluid flow in a collector at 0.2 wt% and 0.3 wt% and at volume flow rates from 30 to 90 L/h. They observed that the collector thermal efficiencies are 53%, 69% and 81% for ethylene glycol, 0.2 wt% and 0.3 wt% of nanofluids, which means there is 30.1% and 52.8% enhancement in collector efficiency compared to ethylene glycol. In the present study with the use of $\phi = 0.3\%$ of Al$_2$O$_3$/water nanofluid, the collector thermal efficiency is enhanced by 22.6% and for $\phi = 0.3\%$ nanofluid with wire coil insert and wire insert pitch of 10 mm, and the collector efficiency is increased by 45.28%. Zamzamian et al. [16] used weight concentrations and in the present study, volume concentrations are used. Moreover, Zamzamian et al. [16] used pure Cu nanoparticles and EG; in the present study, Al$_2$O$_3$ nanoparticles and water are used. The nanoparticles type, particle thermal conductivity, base fluid and concentrations examined by Zamzamian et al. [16] and those investigated in the present study are different, which is the reason for obtaining different collector thermal efficiency enhancements.

4 Conclusion

Al$_2$O$_3$/water nanofluid is used as a working fluid circulating in the collector combined with the coiled wire configurations that have been analyzed experimentally at various particle loadings and flow rates. Based on the thermal efficiency, the collector area, price weight, represented material energy and environmental emissions have been evaluated. The collector efficiency for water is 53%, for 0.3% nanofluid is 65% and

Fig. 24 Comparison of the experimental friction factor versus Re of nanofluid (0.3%) in the solar flat-plate collector with wire coil inserts against the data of Akhavan-Behabadi et al. [38] for MWCNT/water nanofluids
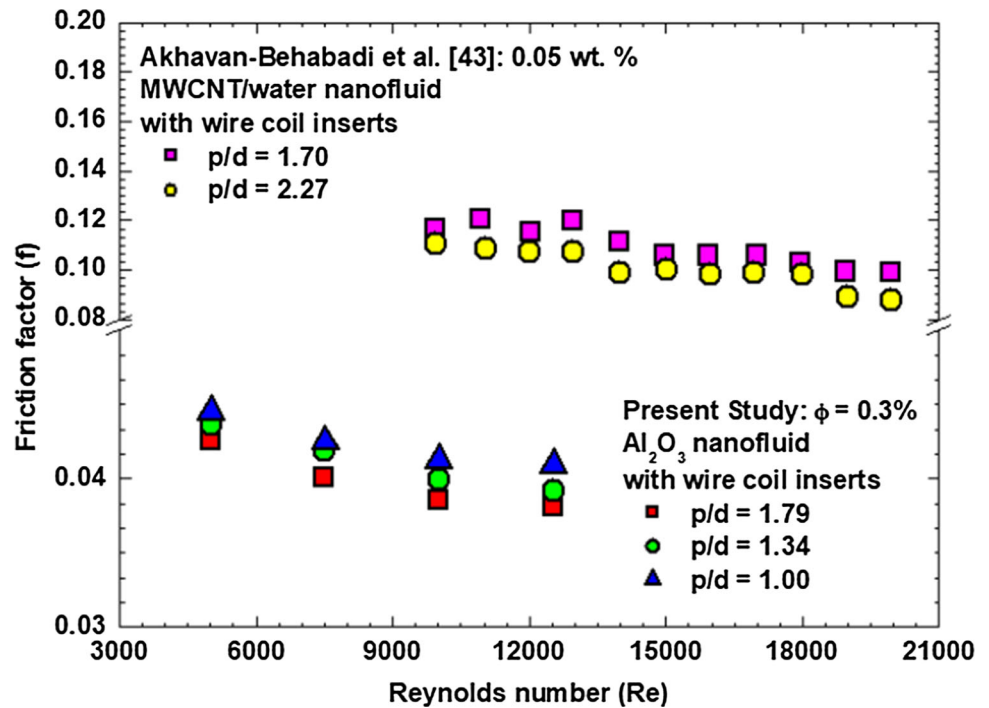
Fig. 25 Experimental friction factor values compared with the proposed friction factor equation values
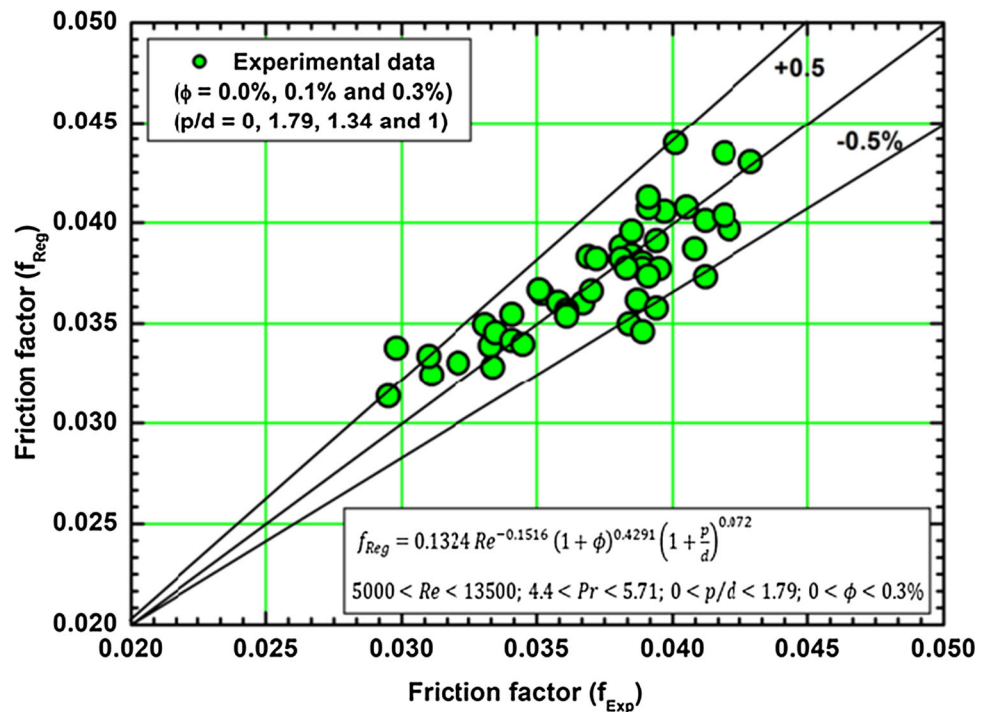
is further enhanced to 77% with the addition of a coiled wire pitch of 10 mm. For circulating nanofluids of 0.1%, 0.2% and 0.3% volume fractions, the area of the collector decreased to 2.74 m², 2.58 m², and 2.44 m², whereas the original area of the collector is 3 m². With the use of nanofluids and addition of coiled wire inserts pitch 10 mm, the collector area further reduced to 2.06 m². The collector cost reduced to 8.66%, 14.02% and 18.67%, with an addition of 0.1%, 0.2% and 0.3% nanofluids, which further decreased to 31.33% by combining nanofluid with 0.3% particle loading and with coiled wire pitch of 10 mm. CO_2 emissions are reduced to 76.32 kg, 123.32 kg and 186.35 kg with the use of 0.1%, 0.2% and 0.3% volume concentrations, which is further reduced to 260.1 kg by using coiled wire pitch of 10 mm insert combined with nanofluid at 0.3% particle loading.

Table 13 The collector efficiency of the present investigation compared with previous studies

Author	Nanofluids	Concentrations	Flow rate (L/h)	Efficiency increase
Sharafeldin et al. [45]	Copper/water	$\phi = 0.03\%$	48	51.0%
Choudhary et al. [6]	ZnO/50:50 EG:W	$\phi = 1.0\%$	60	69.2%
Said et al. [17]	TiO$_2$/water	$\phi = 0.1\%$	90	76.6%
Zamzamian et al. [16]	Cu/EG	0.2 wt%	90	30.1%
		0.3 wt%		52.8%
Sharafeldin and Grof [46]	CeO$_2$	$\phi = 0.066\%$	61.2	10.7%
Ghaderian et al. [47]	CuO/water	$\phi = 0.03\%$	60	32.0%
The present study	Al$_2$O$_3$/water	$\phi = 0.3\%$	300	22.6%
The present study	Al$_2$O$_3$/water	$\phi = 0.3\%$ nanofluid with wire coil insert, $p/d = 1$	300	45.3%

Additionally, the Nusselt number enhanced to 23.22% at 0.3% nanofluid in the collector, which further enhanced to 53.56% with the use of a coiled wire pitch of 10 mm for the same concentration of nanofluid compared to water. The penalty in friction factor with the use of 0.3% nanofluid is 16.94%, and the penalty further enhanced to 38.64% at 0.3% nanofluid with the use of a coiled wire pitch of 10 mm. The nanofluids with coiled wire configurations provided enhanced efficiency, higher heat transfer with negligible friction factor penalty, and also reduced the cost, weight, embodied energy and CO$_2$ emissions.

References

1. Choi, S.U.S.; Eastman, J.A.: Enhanced heat transfer using nanofluids. US Patent 275 6221275 (2001)
2. Yousefi, T.; Shojaeizadeh, E.; Veysi, F.; Zinadini, S.: An experimental investigation on the effect of pH variation of MWCNT–H$_2$O nanofluid on the efficiency of a flat-plate solar collector. Sol. Energy **86**, 771–779 (2012)
3. Yousefi, T.; Veysi, F.; Shojaeizadeh, E.; Zinadini, S.: An experimental investigation on the effect of Al$_2$O$_3$–H$_2$O nanofluid on the efficiency of flat-plate solar collectors. Renew. Energy **39**, 293–298 (2012)
4. Said, Z.; Saidur, R.; Sabiha, M.A.; Hepbasli, A.; Rahim, N.A.: Energy and exergy efficiency of a flat plate solar collector using pH treated Al2O3 nanofluid. J. Clean. Prod. **112**, 3915–3926 (2016)
5. Hussein, O.A.; Habib, K.; Muhsan, A.S.; Saidur, R.; Alawi, O.A.; Ibrahim, T.K.: Thermal performance enhancement of a flat plate solar collector using hybrid nanofluid. Sol. Energy **204**, 208–222 (2020)
6. Choudhary, S.; Sachdeva, A.; Kumar, P.: Influence of stable zinc oxide nanofluid on thermal characteristics of flat plate solar collector. Renew. Energy **152**, 1160–1170 (2020)
7. Tong, Y.; Lee, H.; Kang, W.; Cho, H.: Energy and exergy comparison of a flat-plate solar collector using water, Al2O3 nanofluid, and CuO nanofluid. Appl. Therm. Eng. **159**, 113959 (2019)
8. Polvongsri, S.; Kiatsiriroat, T.: Performance analysis of flat-plate solar collector having silver nanofluid as a working fluid. Heat Transf. Eng. **35**, 1183–1191 (2014)
9. Natarajan, E.; Sathish, R.: Role of nanofluids in solar water heater. Int. J. Adv. Manuf. Technol. (2009). https://doi.org/10.1007/s00170-008-1876-8
10. Otanicar, T.; Phelan, P.E.; Prasher, R.S.; Rosengarten, G.; Taylor, R.A.: Nanofluid based direct absorption solar collector. J. Renew. Sustain. Energy **2**, 033102 (2010)
11. Shojaeizadeh, E.; Veysi, F.; Yousefi, T.; Davodi, F.: An experimental investigation on the efficiency of a flat-plate solar collector with binary working fluid: a case study of propylene glycol (PG)–water. Exp. Therm. Fluid Sci. **53**, 218–226 (2014)
12. Karami, M.; Akhavan-Bahabadi, M.A.; Delfani, S.; Raisee, M.: Experimental investigation of CuO nanofluid-based direct absorption solar collector for residential applications. Renew. Sustain. Energy Rev. **52**, 793–801 (2015)
13. Kiliç, F.; Menlik, T.; Sözen, A.: Effect of titanium dioxide/water nanofluid use on thermal performance of the flat plate solar collector. Sol. Energy **164**, 101–108 (2018)
14. Chaji, H.; Ajabshirchi, Y.; Esmaeilzadeh, E.; Heris, S.Z.; Hedayatizadeh, M.; Kahani, M.: Experimental study on thermal efficiency of flat plate solar collector using TiO$_2$/water nanofluid. Mod. Appl. Sci. **7**, 60–69 (2013)
15. Said, Z.; Saidur, R.; Rahim, N.A.: Energy and exergy analysis of a flat plate solar collector using different sizes of aluminium oxide based nanofluid. J. Clean. Prod. **133**, 518–530 (2016)
16. Zamzamian, A.; Keyanpour Rad, M.; Kiani Neyestani, M.; Jamal-Abad, M.T.: An experimental study on the effect of Cu-synthesized/EG nanofluid on the efficiency of flat-plate solar collectors. Renew. Energy **71**, 658–664 (2014)
17. Said, Z.; Sabiha, M.A.; Saidur, R.; Hepbasli, A.; Rahim, N.A.; Mekhilef, S.; Ward, T.A.: Performance enhancement of a flat plate solar collector using titanium dioxide nanofluid and polyethylene glycol dispersant. J. Clean. Prod. **92**, 343 (2015)
18. Sabiha, M.A.; Saidur, R.; Hassani, S.; Said, Z.; Mekhilef, S.: Energy performance of an evacuated tube solar collector using single walled carbon nanotubes nanofluids. Energy Convers. Manag. **105**, 1377–1388 (2015)
19. Jouybari, H.J.; Saedodin, S.; Zamzamian, A.; Nimvari, M.E.; Wongwises, S.: Effects of porous material and nanoparticles on the thermal performance of a flat plate solar collector: An experimental study. Renew. Energy **114**, 1407–1418 (2017)

20. Mahian, O.; Kianifar, A.; Kalogirou, S.A.; Pop, I.; Wongwises, S.: A review of the applications of nanofluids in solar energy. Int. J. Heat Mass Transf. **57**, 582–594 (2013)

21. Javadi, F.S.; Saidur, R.; Kamalisarvestani, M.: Investigating performance improvement of solar collectors by using nanofluids. Renew. Sust. Energy Rev. **28**, 232–245 (2013)

22. Garcia, A.; Vicente, P.G.; Viedma, A.: Experimental study of heat transfer enhancement with wire coil inserts in laminar-transition-turbulent regimes at different Prandtl numbers. Int. J. Heat Mass Transf. **48**, 4640–4651 (2005)

23. Garcia, A.; Solano, J.P.; Vicente, P.G.; Viedma, A.: Enhancement of laminar and transitional flow heat transfer in tubes by means of wire coil inserts. Int. J. Heat Mass Transf. **50**, 3176–3189 (2007)

24. Garcia, A.; Solano, J.P.; Vicente, P.G.; Viedma, A.: Flow pattern assessment in tubes with wire coil inserts in laminar and transition regimes. Int. J. Heat Fluid Flow **28**, 516–525 (2007)

25. Sundar, L.S.; Bhramara, P.; Ravi Kumar, N.T.; Singh, M.K.; Sousa, A.C.M.: Experimental heat transfer, friction factor and effectiveness analysis of Fe_3O_4 nanofluid flow in a horizontal plain tube with return bend and wire coil inserts. Int. J. Heat Mass Transf. **109**, 440–453 (2017)

26. Abdul Hamid, K.; Azmi, W.H.; Mamat, R.; Sharma, K.V.: Heat transfer performance of TiO_2–SiO_2 nanofluids in a tube with wire coil inserts. Appl. Therm. Eng. **152**, 275–286 (2019)

27. Goudarzi, K.; Jamali, H.: Heat transfer enhancement of Al_2O_3–EG nanofluid in a car radiator with wire coil inserts. Appl. Therm. Eng. (2017). https://doi.org/10.1016/j.applthermaleng.2017.03.016

28. Akyürek, E.F.; Gelis, K.; Sahin, B.; Manay, E.: Experimental analysis for heat transfer of nanofluid with wire coil turbulators in a concentric tube heat exchanger. Results Phys. **9**, 376–389 (2018)

29. Sundar, L.S.; Singh, M.K.; Punnaiah, V.; Sousa, A.C.M.: Experimental investigation of Al_2O_3/water nanofluids on the effectiveness of solar flat-plate collectors with and without twisted tape inserts. Renew. Energy **119**, 820–833 (2018)

30. Sundar, L.S.; Kirubeil, A.; Punnaiah, V.; Singh, M.K.; Sousa, A.C.M.: Effectiveness analysis of solar flat plate collector with Al_2O_3 water nanofluids and with longitudinal strip inserts. Int. J. Heat Mass Transf. **127**, 422–435 (2018)

31. Pak, B.C.; Cho, Y.I.: Hydrodynamic and heat transfer study of dispersed fluids with submicron metallic oxide particles. Exp. Heat Transf. **11**, 151–170 (1998)

32. Einstein, A.: Investigation on Theory of Brownian Motion, 1st edn. Dover publications (1956)

33. Maxwell, J.C.: A Treatise on Electricity and Magnetism, 2nd edn. Oxford University Press, Cambridge (1904)

34. ASHRAE Standard 93–2003, Methods of testing to determine the thermal performance of solar collectors, Atlanta, GA, USA (2003)

35. Whillier, A.: Solar energy collection and its utilization for house heating. Sc. D. Thesis, MIT (1953)

36. Whillier, A.: Design factors influencing collector performance, low temperature engineering. In: Application of Solar Energy, ASHRAE, New York (1967)

37. Hottel, H.C.; Whillier, A.: Evaluation of fat plate collector performance. Trans. Config. Use Solar Energy **2**(1), 74 (1958)

38. Bliss, R.W.: The derivation of several plate efficiency factors useful in the design of flat plate solar heat collectors. Sol. Energy **3**, 55–64 (1959)

39. Ardante, F.; Beccali, G.; Cellura, M.; Brano, V.L.: Life cycle assessment of a solar thermal collector. Renew Energy **30**, 1031–1054 (2005)

40. Faizal, M.; Saidur, R.; Mekhilef, S.; Hepbasli, A.; Mahbubul, I.M.: Energy, economic, and environmental analysis of a flat-plate solar collector operated with SiO_2 nanofluid. Clean Technol Environ. Policy **17**, 1457–1473 (2015)

41. Stalin, P.M.J.; Arjunan, T.V.; Matheswaran, M.M.; Dolli, H.; Sadanandam, N.: Energy, economic and environmental investigation of a flat plate solar collector with CeO_2/water nanofluid. J. Therm. Anal. Calorim. (2019). https://doi.org/10.1007/s10973-019-08670-2

42. Gnielinski, V.: New equations for heat and mass transfer in turbulent pipe and channel flow. Int. Chem. Eng. **16**, 359–368 (1976)

43. Akhavan-Behabadi, M.A.; Shahidi, M.; Aligoodarz, M.R.: An experimental study on heat transfer and pressure drop of MWCNT–water nanofluid inside horizontal coiled wire inserted tube. Int. Commun. Heat Mass Transf. **63**, 62–72 (2015)

44. Blasius, H.: Boundary layers in liquids with low friction. Z. Math. Phys. **56**, 1–37 (1908)

45. Sharafeldin, M.A.; Gróf, G.; Abu-Nada, E.; Mahian, O.: Evacuated tube solar collector performance using copper nanofluid: energy and environmental analysis. Appl. Therm. Eng. **162**, 114205 (2019)

46. Sharafeldin, M.A.; Gróf, G.: Experimental investigation of flat plate solar collector using CeO_2–water nanofluid. Energy Convers. Manag. **155**, 32–41 (2018)

47. Ghaderian, J.; Sidik, N.A.C.; Kasaeian, A.; Ghaderian, S.; Okhovat, A.; Pakzadeh, A.; Samion, S.; Yahy, W.J.: Performance of copper oxide/distilled water nanofluid in evacuated tube solar collector (ETSC) water heater with internal coil under thermo-syphon system circulations. Appl. Therm. Eng. **121**, 520–536 (2017)

48. Saleh, B.; Sundar, L.S.: Thermosyphon flat plate collector with nanodiamond-water nanofluids: properties, friction factor, heat transfer, thermal efficiency, and cost analysis. Arab. J. Sci. Eng. (2021). https://doi.org/10.1007/s13369-021-05371-7

49. Saleh, B.; Sundar, L.S.: Thermal efficiency, heat transfer, and friction factor analyses of MWCNT + Fe_3O_4/water hybrid nanofluids in a solar flat plate collector under thermosyphon condition. Processes **9**, 180 (2021). https://doi.org/10.3390/pr9010180